OPEN ACCESS Freely available online

PLoS one

The Substrate-Driven Transition to an Inward-Facing Conformation in the Functional Mechanism of the Dopamine Transporter

Jufang Shan[1], Jonathan A. Javitch[3,4,5,6], Lei Shi[1,2]*, Harel Weinstein[1,2]*

1 Department of Physiology and Biophysics, Weill Medical College of Cornell University, New York, New York, United States of America, **2** The HRH Prince Alwaleed Bin Talal Bin Abdulaziz Alsaud Institute for Computational Biomedicine, Weill Medical College of Cornell University, New York, New York, United States of America, **3** Center for Molecular Recognition, Columbia University College of Physicians and Surgeons, New York, New York, United States of America, **4** Department of Psychiatry, Columbia University College of Physicians and Surgeons, New York, New York, United States of America, **5** Division of Molecular Therapeutics, New York State Psychiatric Institute, New York, New York, United States of America, **6** Department of Pharmacology, Columbia University College of Physicians and Surgeons, New York, New York, United States of America

Abstract

Background: The dopamine transporter (DAT), a member of the neurotransmitter:Na^+ symporter (NSS) family, terminates dopaminergic neurotransmission and is a major molecular target for psychostimulants such as cocaine and amphetamine, and for the treatment of attention deficit disorder and depression. The crystal structures of the prokaryotic NSS homolog of DAT, the leucine transporter LeuT, have provided critical structural insights about the occluded and outward-facing conformations visited during the substrate transport, but only limited clues regarding mechanism. To understand the transport mechanism in DAT we have used a homology model based on the LeuT structure in a computational protocol validated previously for LeuT, in which steered molecular dynamics (SMD) simulations guide the substrate along a pathway leading from the extracellular end to the intracellular (cytoplasmic) end.

Methodology/Principal Findings: Key findings are (1) a second substrate binding site in the extracellular vestibule, and (2) models of the conformational states identified as occluded, doubly occupied, and inward-facing. The transition between these states involve a spatially ordered sequence of interactions between the two substrate-binding sites, followed by rearrangements in structural elements located between the primary binding site and the cytoplasmic end. These rearrangements are facilitated by identified conserved hinge regions and a reorganization of interaction networks that had been identified as gates.

Conclusions/Significance: Computational simulations supported by information available from experiments in DAT and other NSS transporters have produced a detailed mechanistic proposal for the dynamic changes associated with substrate transport in DAT. This allosteric mechanism is triggered by the binding of substrate in the S2 site in the presence of the substrate in the S1 site. Specific structural elements involved in this mechanism, and their roles in the conformational transitions illuminated here describe, a specific substrate-driven allosteric mechanism that is directly amenable to experiment as shown previously for LeuT.

Citation: Shan J, Javitch JA, Shi L, Weinstein H (2011) The Substrate-Driven Transition to an Inward-Facing Conformation in the Functional Mechanism of the Dopamine Transporter. PLoS ONE 6(1): e16350. doi:10.1371/journal.pone.0016350

Editor: Vladimir Uversky, University of South Florida College of Medicine, United States of America

Received October 27, 2010; **Accepted** December 13, 2010; **Published** January 27, 2011

Funding: This work was supported by National Institutes of Health grants from the National Institute on Drug Abuse (DA012408, DA023694, DA022413, and DA17293). The funders had no role in study design, data collection and analysis, decision to publish, or preparation of the manuscript.

Competing Interests: The authors have declared that no competing interests exist.

* E-mail: les2007@med.cornell.edu (LS); haw2002@med.cornell.edu (HW)

Introduction

The dopamine transporter (DAT) is a member of the neurotransmitter:Na^+ symporter (NSS) family that includes the transporters for other biogenic amines (serotonin and norepinephrine), amino acids (GABA, glycine, proline, taurine) and osmolytes (betaine, creatine) [1]. DAT terminates dopaminergic neurotransmission by transporting dopamine (DA) against its concentration gradient from the synaptic cleft into the pre-synaptic neuron in a Na^+ and Cl^- dependent process. DAT is recognized as the primary target of psychostimulants such as cocaine and amphetamine, and has been implicated in multiple disorders, including Attention-Deficit Hyperactivity Disorder and depression.

Structure-function relations have been studied extensively for DAT using both site-directed and deletion mutagenesis, as well as cross-linking, engineering of metal binding sites, and substituted-cysteine accessibility approaches (see [2–9] and references therein). However, the molecular details of the dynamic transport mechanism remain elusive. The high resolution structures of LeuT [10–15], a prokaryotic homolog of DAT, have provided essential structural insights that can serve to interpret the results of experimental investigations of DAT in a structural context [16], but offer only limited clues about the molecular mechanism of transport. In the first LeuT structure, the substrate is located in the center of protein, occluded from both the periplasmic and the

cytoplasmic milieus. Although the breakthrough structural information about LeuT [10–15], and about some other related transporters [17–19] is recent, a number of models have been proposed for the functional mechanism of LeuT and cognate NSS transporters. For example, the model proposed by Gouaux et al. involves two additional conformations, outward-facing and inward-facing [15], which is in line with the alternating access model for transporters proposed earlier [20]. Structural modeling supported by experimental probing has offered ideas based on the symmetry features of the molecules in this family [21,22], and the powerful approach of computational simulation using high resolution structural information was applied to the exploration of the functional mechanisms of proteins with a LeuT-like structure fold (e.g., see [10,16,23–33]. The current mechanistic understanding emerging from the combined experimental and computational studies, while still incomplete, suggests that the functional mechanisms of the human neurotransmitter transporters in the NSS family are much more complex than would be suspected from the canonical "alternating-access model" of the transition between an outward-facing and an inward-facing form [34].

A central motif of these complex mechanisms is the allosteric effect of ion- and substrate-binding on the translocation process. Both computation and experiment suggest that in LeuT these binding events trigger a series of local perturbations that are propagated from one end of the transporter to the other, generating significant changes in the preferred state [29,34]. The large-scale structural changes are interpretable as the formation of outward- and inward-open conformations supporting the transport process. One element of the allosteric mechanism that produces the conformational changes through propagation of local perturbations, rather than large rigid body motions, is the effect of ligand binding in the extracellular vestibule of LeuT, termed the S2 binding site [29]. Using binding and flux experiments we had shown that the primary binding site (S1 site) and the S2 site could be occupied by substrate simultaneously, and that substrate in the extracellular vestibule S2 site could allosterically trigger intracellular release of Na^+ and substrate from the S1 site, thereby functioning as a "symport effector" [29]. The S2 site also binds tricyclic antidepressants (TCAs) [11], which interact differently from the substrate and do not promote substrate release from the S1 site, thereby acting as symport uncouplers that inhibit transport [11]. In addition, we identified from computational analyses of the LeuT structures the nature of rearrangements in the extracellular region that differentiate the actions of substrates from inhibitors bound in the S2 site [10]. The likely structural commonalities among the transmembrane (TM) domains of LeuT and eukaryotic NSS [35,36] suggest that many of the details elucidated thus far for LeuT will be shared within this protein family. Other details will differ, however, leading to important functional distinctions in selectivity, sensitivity and responses to substrates, ions and various ligands, such as those evidenced among the human neurotransmitter transporters.

For DAT, previous molecular dynamics (MD) simulations have identified structural elements important for substrate binding and the formation of an occluded state [37,38]. However, the involvement of a LeuT-like S2 binding site and any mechanistic role that an S2-bound substrate might have in modulating DAT function in the manner described for LeuT, remain open questions that are examined here in the context of the allosteric mechanism responsible for conformational transitions in DAT. To study the mechanism of substrate translocation to the intracellular side we used a DAT model described previously [39] to explore the pathway with steered molecular dynamics (SMD) simulations as had been done previously for LeuT [29,40] and other transporters [33,41]. Here, this protocol was augmented with the addition of long MD equilibrations of the various DAT states, to determine properties and function-related dynamics of the S1 and S2 sites, as well as the permeation pathway and function-related states of the transporter molecule. We addressed for the first time the (i)-the molecular mechanism of communication between the S1 and S2 sites, and (ii)-the structural and dynamic elements that enable the DAT molecule to open towards the cytoplasm, which allowed us to identify structural elements responsible for the propagation of the conformational changes. These are shown here to consist, respectively, of specific residues positioned between the S1 and S2 sites, and a cluster of aromatic residues positioned below the S1 site toward the intracellular end. The conformational rearrangements are shown to involve specific "hinge residues" in the transition between the occluded and the inward-facing states. We report on remarkable agreement between the identities of the key components in the translocation mechanism we are able to identify from the simulations and experimental data in the literature. Together, these results achieve a comprehensive molecular identification of key elements of the substrate translocation pathway and the underlying allosteric mechanism in DAT, at a level of detail that is directly amenable to further experimental validation.

Results and Discussion

I. The S1 and S2 binding sites and the substrate translocation pathway of DAT

To investigate the translocation mechanism of DAT we performed SMD simulations (see Methods for details) on a homology model that we had constructed previously and simulated in explicit water and lipid environment [39]. This model of DAT in the occluded state (termed here S1-DAT) is based on the LeuT template [15] and the characterization of the Cl^- binding site [42], and includes in the S1 site one dopamine (DA) substrate molecule, two Na^+ and one Cl^- ions. DA was docked in the S1 site by aligning its amine and hydrophobic portion with those of the leucine in the crystal structure of LeuT (see Methods for details). The permeation pathway from the extracellular side was explored in this model with SMD simulations pulling DA from the S1 site towards the extracellular side. Much like in LeuT [29], this procedure identified here a second binding site in a region above (extracellular to) the S1 site by the behavior of the steering force experienced when pulling DA that was the same as described previously for the equivalent simulation in LeuT. The force profile (see especially Figure S1 in File S1, in [29]) suggests the presence of an extracellular pocket similar to the S2 site detected computationally and validated experimentally in LeuT at a similar position [29]. After equilibrating a substrate in this S2 site, a second DA molecule was added and positioned in the S1 site, and the dual substrate configuration (S1,S2-DAT) was equilibrated for 25 ns (Figure 1A,C).

To explore the intracellular permeation pathway, two independent SMD simulations were initiated from S1,S2-DAT. After DA from the S1 site reached the intracellular side, the system was further equilibrated with 15 ns MD simulation in each of them. The two separate runs converged to the same final inward-facing conformation. In the following sections, we delineate our characterization of the S1 and S2 sites and the substrate translocation pathway based on the analysis of three equilibrated conformational states, namely, S1-DAT, S1,S2-DAT and the inward-facing conformation.

The S1 and S2 binding sites. The residues forming the S1 site were identified from the equilibration trajectories of both S1-DAT and S1,S2-DAT as those close to the substrate during the simulation

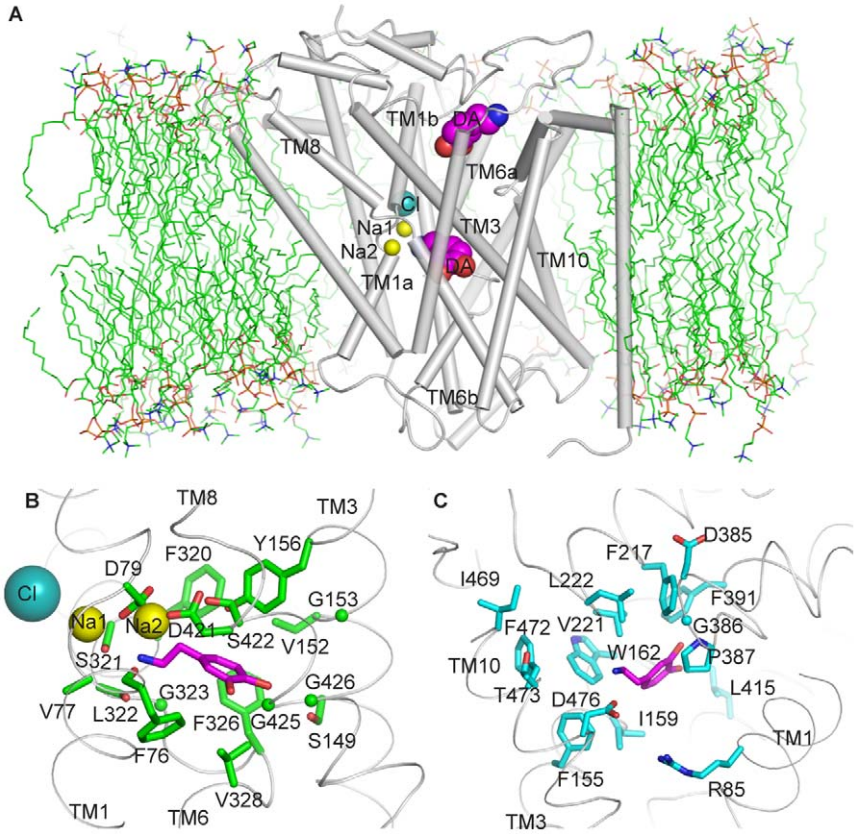

Figure 1. The substrate binding sites of DAT. (**A**) S1,S2-DAT with DA in both the S1 and S2 sites, immersed in a lipid bilayer. The S1 site is located in the middle of the TM bundle and the S2 site is located ~ 10 Å above the S1 site. (**B**) DA in the S1 site interacts with residues from TMs1, 3, 6 and 8 (viewing perspective is similar to that in (**A**)). (**C**) DA in the S2 site interacts mainly with residues from TMs1, 3 and 10, EL2, and EL4 (viewed from the exit of the extracellular vestibule).
doi:10.1371/journal.pone.0016350.g001

trajectories (Figure 1A,B). The resulting binding pose of the DA substrate in the S1 site is consistent with previous studies [37,38,43]. Most residues in contact with the S1 substrate were from TMs1, 3, 6 and 8 and remained the same in both trajectories (Figure 1B, Table 1). However, the identities and the orientations of several S1 residues were different when assigned in the presence or absence of substrate in the S2 site (Figure 2B, Table 1), suggesting that S2 binding has an allosteric effect on the S1 site (see below).

The S2 site residues identified in the equilibration trajectory of S1,S2-DAT were from TMs1, 3, and 10, and the extracellular loops EL2 and EL4 (Figure 1C, Table 2). The composition of the S2 site in DAT is similar to that in LeuT [29], and includes the corresponding (aligned) hydrophobic residues $F155^{3.49}$, $I159^{3.53}$, $W162^{3.56}$, and $F472^{10.44}$ and a pair of corresponding charged residues, $D476^{10.48}$ and $R85^{1.51}$. Note, however, that EL2 is much longer in eukaryotic NSS than in LeuT, and is involved in the S2 site of the DAT model, but not in the S2 site of LeuT.

The permeation pathway. Residues contacted as the substrate moved from the S1 site outward toward the S2 site during the SMD/MD simulation were classified as belonging to the extracellular transport pathway that is lined by two layers of hydrophobic residues along TMs1, 3, 8 and 10 (Table 3). Following the same criterion, residues in contact with the substrate as it moved from the S1 site toward the cytoplasmic side in the two independent SMD simulations, were similarly classified as belonging to the intracellular translocation pathway lined mainly by residues from TMs1, 5, 6 and 8 (Table 4).

The endpoint for SMD pulling in the intracellular pathway was determined by monitoring the interaction energy between DA and solvating water molecules. In the S1 site the water-DA interaction energy was ~ −19 kcal/mol, reflecting minimal direct contact. The water-DA interaction became stronger as the substrate moved toward the cytoplasm, indicating increasing solvation until DA established an equilibrated interaction with the conserved $E428^{8.66}$, when the interaction energy stabilized at ~ −60 kcal/mol suggesting full solvation by surrounding waters; this was supported by visual inspection. SMD pulling was terminated at this position. Notably, the residue corresponding to $E428^{8.66}$ in various transporters has been shown to be important for substrate transport [44,45] and shown to become solvent exposed in the inward-facing conformation of GAT-1 [45]. The observed interaction between DA and $E428^{8.66}$ suggests that this functionally important glutamate may be an anchoring point along the transport pathway where the substrate makes stable interactions before it moves to the cytoplasm, or reversely in the initial step of efflux.

II. Substrate binding in the S2 site prepares DAT for the transport of dopamine

The changes observed in the S1 site when substrate is present in the S2 site suggest a mode of allosteric interaction between the binding sites. The elements of this allosteric mechanism are the coordinated rearrangements of key residues and structural elements (TM segments and loops) discussed below.

Table 1. Composition of the S1 site.

Index	Residue	Cα-z[a]	S1-DAT %[b]	S1,S2-DAT %[c]
1.42	F76	−1.24	100	100
1.43	A77	0.78	99	99
1.45	D79	5.32	100	100
3.43	S149	0.39	8	20
3.46	V152	5.11	99	18
3.47	G153	3.19	23	0
3.50	Y156	6.30	95	95
6.53	F320	5.58	100	100
6.54	S321	5.64	100	100
6.55	L322	2.00	99	100
6.56	G323	1.16	100	100
6.59	F326	−1.28	99	98
6.61	V328	−4.64	73	100
8.59	D421	−0.98	0	20
8.60	S422	1.13	100	100
8.61	A423	1.73	24	0
8.63	G425	−3.18	19	100
8.64	G426	−1.17	98	99

[a]The z-coordinates for residues at the S1 site of DAT. S1-DAT equilibrated at 14 ns was used for the analysis since it is the starting structure for pulling DA towards the extracellular side.
[b]The percentage of time spent by the residue within 3.5 Å of DA (see Methods) during the 6–16 ns segment of equilibration of the S1-DAT model.
[c]The percentage of time spent by the residue within 3.5 Å of DA during the 6–25 ns segment of equilibration of the S1,S2-DAT model.
doi:10.1371/journal.pone.0016350.t001

An allosteric interaction network between the S1 and S2 sites. The presence of substrate in the S2 site is associated with a downward repositioning of the center of mass of the S1-bound substrate by 1 Å (Figure 2A,B). This is accompanied by the dissociation of several DA-protein contacts, and the formation of new ones (Figure 2B). Comparison of the equilibrated S1-DAT and S1,S2-DAT models showed that the downward repositioning is enabled by the rearrangement of (i)-several conserved hydrophobic residues within the S1 site, or in between the S1 and S2 sites (e.g., the significant changes of F76$^{1.42}$, Y156$^{3.50}$ and F320$^{6.53}$ shown in Figure 2B), and (ii)-the interposed water molecules. The rearrangement involved in the S1/S2 allosteric interaction is accomplished by a set of highly conserved residues that are not sequential in the primary structure, but form a network in space as indicated in Figure 2.

Compared to S1-DAT, which corresponds to the LeuT crystal structure, in the S1,S2-DAT model the EL2 and EL4 loops have moved towards the S2 substrate and pushed the extracellular segment of TM3 inward to the S2 site (see Figure S1 in File S1). This appears to cause conformational changes in the S1 site, propagated through a conserved interaction network (Table S1 in File S1). The dynamic sequence of events has I390^{EL4} and F391^{EL4} pushing the sidechain of W84$^{1.50}$, and then of L80$^{1.46}$ down toward the S1 site (Figure 2C). As a result, the sidechains of Y156$^{3.50}$ and F320$^{6.53}$ that are located between the S1 and S2 sites and have their phenyl rings above the catechol moiety of DA, rotated to push downward on the ligand in the S1 site. F155$^{3.49}$ facilitated the rotation of Y156$^{3.50}$ in a rearrangement that is likely due to its interaction with the substrate in the S2 site. Thus, the communication between the S1 and S2 sites appears to depend on this sequence of rearrangements of the highly conserved set of hydrophobic and aromatic residues (L80$^{1.46}$, W84$^{1.50}$, F155$^{3.49}$, Y156$^{3.50}$, F320$^{6.53}$, I390^{EL4} and F391^{EL4}).

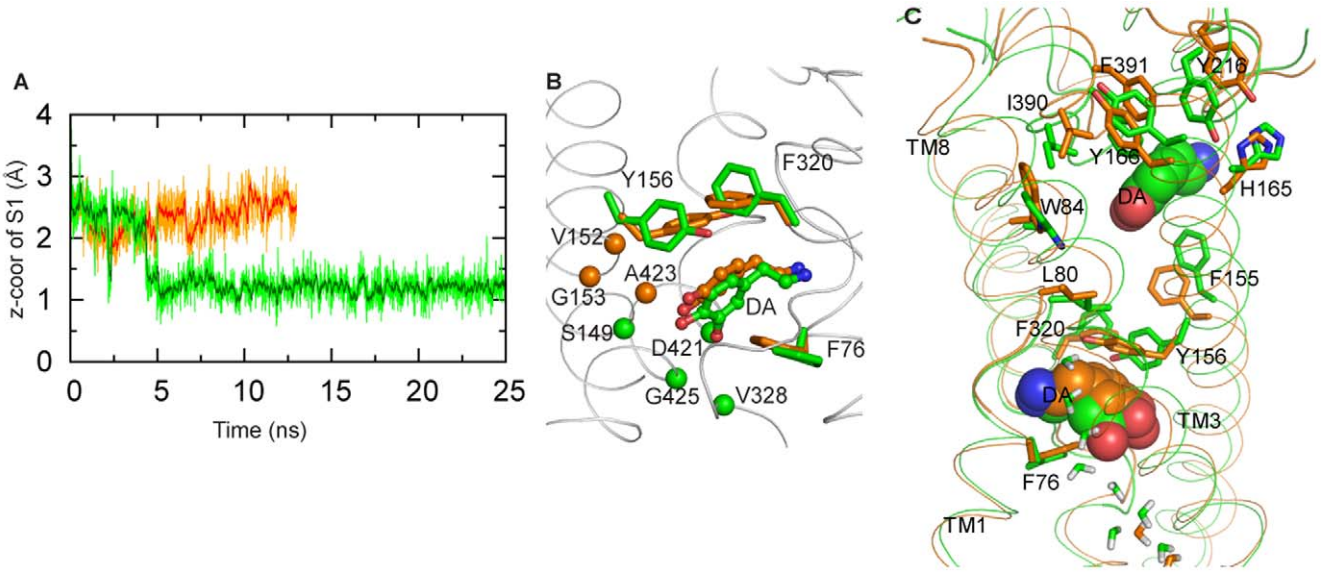

Figure 2. The allosteric effect of S2 on the S1 site. (**A**) Change in position of the DA substrate in the S1 site during equilibration of the S1,S2-DAT model. The green trace shows that the Z-coordinate of DA (center of mass) decreases by ~ 1.5 Å (i.e., DA is shifted downward toward the intracellular side), compared to its position in S1-DAT (orange trace). (**B**) The positional changes of DA, the rotamer changes of F76$^{1.42}$, Y156$^{3.50}$ and F320$^{6.53}$, and the changes in the composition of the S1 site in S1-DAT (residues rendered in orange) compared to S1,S2-DAT (in green). Note that in S1,S2-DAT, the substrate interacts more (i.e., a higher percentage of time) with S149$^{3.43}$, V328$^{6.61}$, and G425$^{8.63}$, and establishes a new interaction with D421$^{8.59}$ (C_α atoms shown as orange spheres) while losing interactions with V152$^{3.46}$, G153$^{3.47}$ and A423$^{8.61}$ (C_α atom shown as green spheres). (**C**) The residues forming an interaction network involved in conformational transitions between S1-DAT (orange) and S1,S2-DAT (green). Residues I390^{EL4} and F391^{EL4} are in contact with DA in the S2 site. Note that changes in W84$^{1.50}$, L80$^{1.46}$, Y156$^{3.50}$ and F320$^{6.53}$ are coordinated with I390^{EL4} and F391^{EL4} (Table 1).
doi:10.1371/journal.pone.0016350.g002

Table 2. Composition of the S2 site.

Index	Residue	Cα-z[a]	S1,S2-DAT -Average %[b]	Inward -Average %[c]
1.51	R85	14.00	30	1
3.49	F155	8.26	90	92
3.53	I159	10.20	45	97
3.56	W162	13.55	93	99
EL2	F217	25.71	51	94
	V221	21.92	98	98
	L222	23.71	94	53
EL4	D385	26.11	22	0
	G386	22.68	31	2
	P387	20.82	80	100
	F391	23.47	19	4
8.53	L415	11.26	3	98
10.41	I469	20.78	30	34
10.44	F472	16.09	71	0
10.45	T473	18.04	49	0
10.48	D476	14.19	99	100

[a]as in Table1.
[b]The percentage of time spent by the residue within 3.5 Å of DA (see Methods) during the 6–25 ns of equilibration of the S1,S2-DAT model.
[c]The percentage of time spent by the residue within 3.5 Å of DA during the 6–15 ns of equilibration of the inward-facing model.
doi:10.1371/journal.pone.0016350.t002

Indeed, the difference distance matrix map (Fig. S1 in File S1) shows that residues $L80^{1.46}$, $W84^{1.50}$, $I390^{EL4}$ and $F391^{EL4}$ moved together with $F155^{3.49}$, $Y156^{3.50}$ or $F320^{6.53}$. This type of allosteric communication function carried out by a conserved network in the molecular space had been proposed for allosteric networks in other molecular systems as well, e.g., in PDZ domains and other proteins [46–48].

The functional role of the rearrangements we observed extends to a change in the coordination of Na2 in the S1,S2-DAT model, which may well be associated with the release of the ion in a process observed both computationally and experimentally for LeuT, as described in [29]. Compared to the S1-DAT, in the S1,S2-DAT model the backbone carbonyl of $L418^{8.56}$ is flipped, with a 130° change in its ψ angle (Table S1 in File S1), so that it no longer coordinates Na2 (Figure S1G in File S1) but interacts instead with $W84^{1.50}$ (through a water molecule), which stabilizes it in a new position. With this set of rearrangements, the middle portion of TM8 near $L418^{8.56}$ moves back from the Na2 site and away from TM1, facilitating the observed rotamer changes in $L80^{1.46}$ and $Y156^{3.50}$.

Table 3. The substrate translocation pathway from the S1 site to the S2 site.

Index	Residue	Cα-z[a]	Max %[b]
1.46	L80	8.96	100
1.47	A81	9.50	100
1.50	W84	14.00	55
3.57	A163	12.42	27
EL4	I390	20.48	10
10.49	H477	14.84	5
10.51	A479	10.00	76
10.52	A480	12.12	100

[a]as in Table 1.
[b]For SMD calculations, percentages were defined as the number of frames during which substrate sees a residue/(Frame No. when it last sees that residue - Frame No. when it first sees that residue); both the SMD and MD equilibrations were included for the calculation. The maximum percentages from individual SMD or MD simulations are reported.
doi:10.1371/journal.pone.0016350.t003

Table 4. The substrate translocation pathway from the S1 site to the intracellular site.

Index	Residue	Cα-z [a]	Max (1^{st}/2^{nd}) % [b]
1.25	R60	−20.47	69/44
1.29	W63	−14.34	99/94
1.38	S72	−6.59	1/100
1.41	G75	−1.70	1/24
2.66	A128	−9.93	56/25
4.62	L255	−7.14	59/0
4.65	G258	−10.61	0/35
5.36	V259	−11.44	98/70
5.40	S262	−7.22	63/81
5.41	G263	−8.90	16/27
5.43	V266	−3.55	94/97
6.62	L329	−6.63	16/0
6.64	A331	−9.52	100/100
6.65	F332	−9.81	100/100
6.68	Y335	−15.58	100/100
8.62	M424	−1.90	51/47
8.66	E428	−6.11	100/100
8.67	S429	−5.48	78/84
8.70	T432	−8.97	3/66
8.71	G433	−9.56	11/58
8.74	D436	−14.31	7/44
9.38	R445	−13.45	1/50

[a]as in Table 1.
[b]as in Table 3. The results are shown as the percentage from the first simulation/percentage from the second simulation.
doi:10.1371/journal.pone.0016350.t004

The allosteric effect of S2 binding induces an open-inward conformation allowing water penetration. We found that the formation of continuous water pathways in the core of DAT (Figure 3) is associated dynamically with substrate binding in the S2 site. The pathway determined from the SMD simulations for the exit of substrate from the S1 site corresponds exactly to a water channel (Table 4), thus identifying a specific mechanism for substrate binding in the S2 site to trigger permeation. Notably, the residues in the highly conserved aromatic cluster lining this channel, which we observe in the simulations to coordinate the movement of DA, are buried in the core of the transporter in the S1-DAT state. However, when S2-bound DA triggers the formation of the channel, part of this aromatic cluster ($F69^{1.35}$, $F76^{1.42}$ and $F332^{6.65}$) becomes more solvated (Figure S2 in File S1), supporting the relation between substrate binding in the S2 site and the opening of the intracellular pathway for the penetration of water and the downward

movement of the substrate from the S1 site. Correspondingly, the interaction energy of the S1-bound substrate with water is ~ −10 kcal/mol in the absence of S2-bound substrate, but becomes much stronger (~−19 kcal/mol) when substrate occupies the S2 site due to water penetration that also facilitates the process of release into the cytoplasmic medium (Figure 3E). This is enabled by rotamer changes of the buried $S262^{5.40}$ and $M424^{8.62}$ residues in the core of the protein in S1,S2-DAT (Table S1 in File S1), which make room for waters to move up from the intracellular side (Figure 3F,G). Further, the change in conformation of $F76^{1.42}$ (see above) induced $S422^{8.60}$ to move toward $Y156^{3.50}$ (Figure 3F,G), resulting in the disruption of the interaction between $S422^{8.60}$ and $F76^{1.42}$ and water penetration into the S1 site. Notably, Na2 is solvated in this process (facilitating its inward release as described in our findings for LeuT [29]), whereas Na1 remains fully secluded from water.

Release of DA from the S1 site involves specific changes in a conserved cluster of aromatic residues. We found that ligand binding in the S2 site triggers remarkable changes in the putative permeation pathway of DAT, but the subsequent inward movement of DA from the S1 site toward the intracellular exit involves additional conformational rearrangements in a cluster of highly conserved aromatic residues in TMs1a and 6b (Table S2 in File S1) that includes $F69^{1.35}$, $F76^{1.42}$, $F332^{6.65}$, as well as $W63^{1.29(NT)}$ and $Y335^{6.68}$ (Figure 4A). A set of sequential rotamer changes in these residues is propagated through a series of local conformational rearrangements in the intracellular segments of the TMs. The changes in the rotamers of $F76^{1.42}$, $F332^{6.65}$ and $Y335^{6.68}$ along the translocation pathway (Figure 4B), are correlated (Figure S3 in File S1), as indicated by the application of Spearman's rank test [49] to the trajectory-derived data from the SMD simulations of substrate moving inward from the S1 site. Specifically, rotamer changes in $F76^{1.42}$ and $F332^{6.65}$ allow DA to exit from the S1 site (Figure 4C,D), and rotation of $F332^{6.65}$ produces the rearrangement of $F69^{1.35}$ that results in the significant movement of the intracellular end of TM1a away from TM6b (Figure 4D). Finally, $Y335^{6.68}$ dissociates from an H-bond interaction with $E428^{8.66}$, enabling further movement in TM1a and the N-terminus, which includes $W63^{1.29(NT)}$ (Figure 4E,F). Overall, the conformational changes within the entire aromatic cluster produce an opening surrounded by TMs 1, 5, 6 and 8 that enables water penetration, as indicated by the significant increase in the values of solvent accessible surface areas (SASA) calculated for the dynamics trajectories for residues $F332^{6.65}$, $Y335^{6.68}$ and $W63^{1.29(NT)}$ in a time sequence corresponding to the direction of the pathway (Figure 4B).

The dynamic mechanism emerging from our SMD and MD simulations indicated that the rearrangements of $F76^{1.42}$, $F332^{6.65}$ and $Y335^{6.68}$ in the aromatic cluster, together with $E428^{8.66}$, function as "gates" along the intracellular translocation pathway. The first of these gates is composed of $F76^{1.42}$ and $F332^{6.65}$ (Figure 4C,D) and thus hydrophobic in nature. When the sidechains of the two residues rotate away from the translocation pathway, DA is able to move downward and leave the S1 site. The second gate involves $Y335^{6.68}$ and $E428^{8.66}$ connected by an H-bond. When $Y335^{6.68}$ rotates and the H-bond breaks (Figure 4E,F), DA can move further down the intracellular end of the DAT protein, where it becomes fully solvated. These multi-residue gates open due to coordinated changes in the rotamers of the residues in the aromatic cluster (discussed above) and their neighbors, underscoring the key role of this highly conserved cluster of aromatic residues ($W63^{1.29(NT)}$, $F69^{1.35}$, $F76^{1.42}$, $F332^{6.65}$ and $Y335^{6.68}$) in the conformational transition between different functionally-related states of the transporter protein. This is similar to the aromatic cluster found in TMs 5–6 of Class A GPCRs that is known to contribute to switching between inactive and active states of the receptor (e.g., see [50–52]).

III. Global rearrangement from S1-DAT to the inward-facing conformation

The ordered sequence of local structure perturbations described above gives rise to a global conformational rearrangement of the transporter molecule from one state (e.g., S1-DAT) to another (e.g., inward-facing). A structural characterization of this transition to the inward-facing conformation was obtained with the RMSDTT algorithm [53] that performs an iterative alignment of structures, giving larger weight to regions that have small residue-based RMSDs. Comparing S1-DAT to the inward-facing conformation, this procedure showed that as the intracellular passage opened for the substrate DA, portions of TM segments positioned extracellular to the S1 site have small residue-based backbone RMSDs (1–2 Å), whereas the TM segment portions ranging from the S1 site downward to the intracellular side exhibited drastic conformational changes, with RMSDs of 3–6 Å (Figure S4 and Table S3 in File S1). The same structural characterization of the transition was observed when the models of the two DAT states were aligned using two other approaches, either aligning residues in the conserved TMs1, 3, 6 and 8, or performing 3-D structural alignment of entire DAT structures ("Stamp structural alignment" in VMD [54,55]).

The global conformational rearrangement at the extracellular side caused by the S2-bound substrate is small, but noticeable. TM3 residues $F155^{3.49}$, $I159^{3.53}$ and $W162^{3.56}$ are in direct contact with the ligand in the inward-facing conformation and alter the nearby TM packing, so that TM4 moves toward TM3, and TM8 tilts outward to TMs3 and 4 (Figure 5A). Both EL2 (connecting TMs3 and 4) and EL4 (connecting TMs7 and 8) move downward to interact with the ligand and close the S2 site. In addition, EL3 (between TMs5 and 6) also moves inward toward the bundle, consistent with the movement of EL3 observed in LeuT [10,34,56].

Conformational rearrangements at the intracellular side make room for the descending DA: TMs1, 4, 5, 8, and 9 move as one group, and TMs2, 6, 7, 10, and 11 as a second group that distances itself from the first. Notably, TM1 exhibits the largest movement, consistent with experimental data for LeuT [34]. TMs3 and 12 move to fill in the space created by the rearrangements of the two groups (Figure 5B), so that TM3 moves towards the position originally occupied by the second group to maintain its associations with TMs6 and 10, and TM12 to maintain contacts with TMs3, 8 and 9.

Overall, we found the global rearrangements in DAT to be similar to those observed from the comparison of the LeuT crystal structure of the occluded form [15] to the inward-facing LeuT model obtained from SMD [57], with the difference that in LeuT some intracellular portions of TM segments exhibited either smaller-scale movements (TMs4 and 8) or did not move at all (TMs3, 9 and 10). This difference may well be due to the higher rigidity that LeuT, which is from a hyperthermophilic organism, would be expected to exhibit at the simulated room temperature; the rigidity is likely to be achieved by a combination of several factors [58].

Hinge regions enable the global conformational transitions. That specific hinge regions enable the dynamics of propagation of the observed allosteric effects was established first for the unwound regions of TMs1 and 6. In the transition from S1-DAT to the inward-facing conformation, the extracellular end segments of TM1 (TM1b) and TM6 (TM6a) (above the

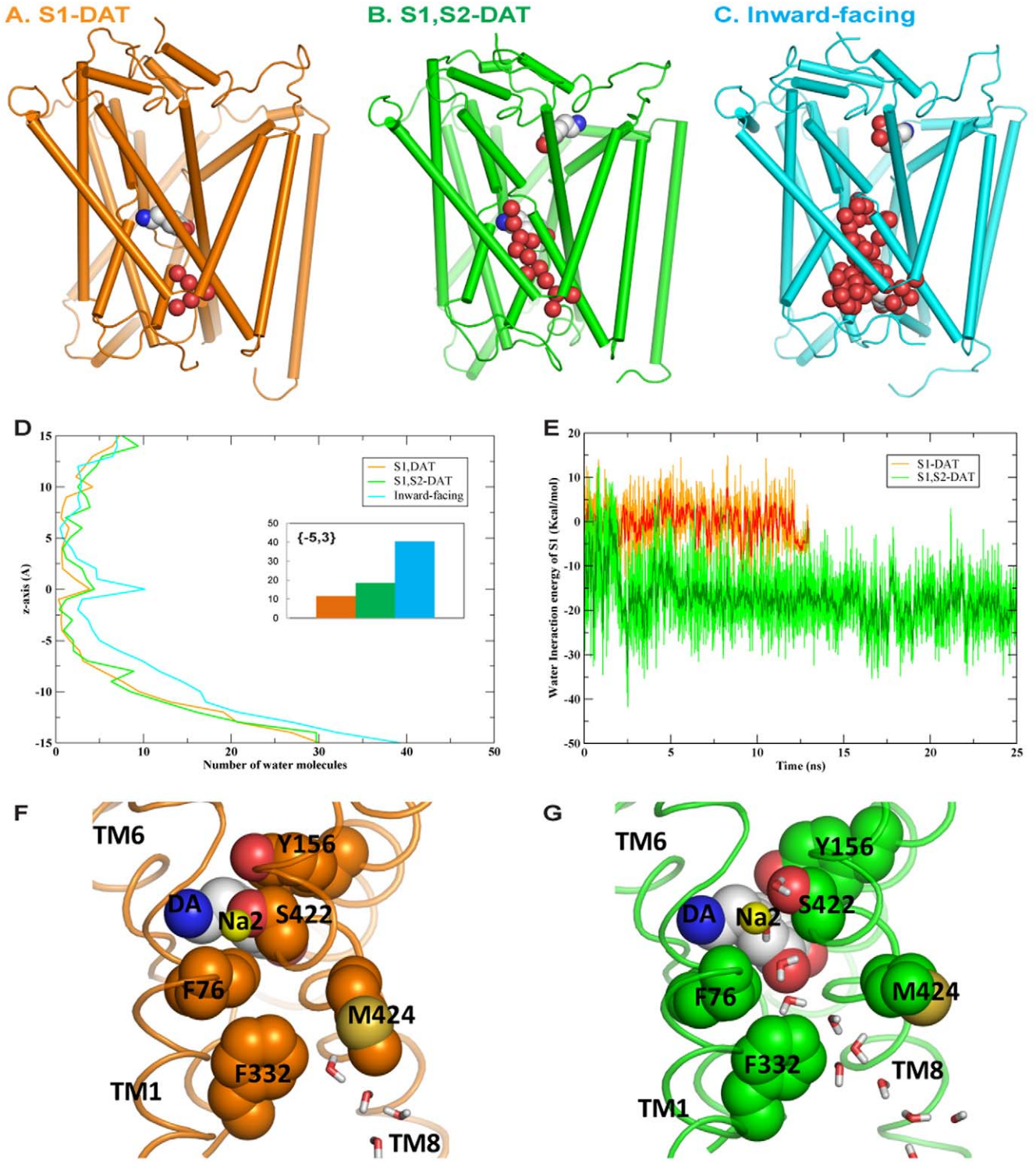

Figure 3. The S2-induced transition of DAT to an inward-open conformation is accompanied by water penetration. (**A**, **B**, **C**) Waters (red balls) gradually penetrate to the S1 site, during the transition from S1-DAT (**A**) to S1,S2-DAT (**B**), then to the inward-facing conformation (**C**). (**D**) Average number of waters along the membrane normal (the z-axis; z = 0 is at the center of the membrane) in (**A**)–(**C**). The insert shows waters accumulated between −5 Å and +3 Å (z-axis) in the corresponding models identified by the colors. (**E**) DA in the S1 site interacts more favorably with waters in the presence of a substrate in the S2 site (green) than in the absence of a substrate in the S2 site (orange). (**F**) and (**G**) show magnified details of (**A**) and (**B**), respectively, with the same color coding and water in stick representations.
doi:10.1371/journal.pone.0016350.g003

unwound region) remain largely unchanged, whereas the intracellular ends, TMs1a and 6b, swing outward non-symmetrically to open the substrate translocation pathway. TM1a moves substantially more, thereby distancing itself from TM6b (Figure 5C). Consistent with the mechanism proposed from the crystal structure of LeuT [15], we did not observe a big

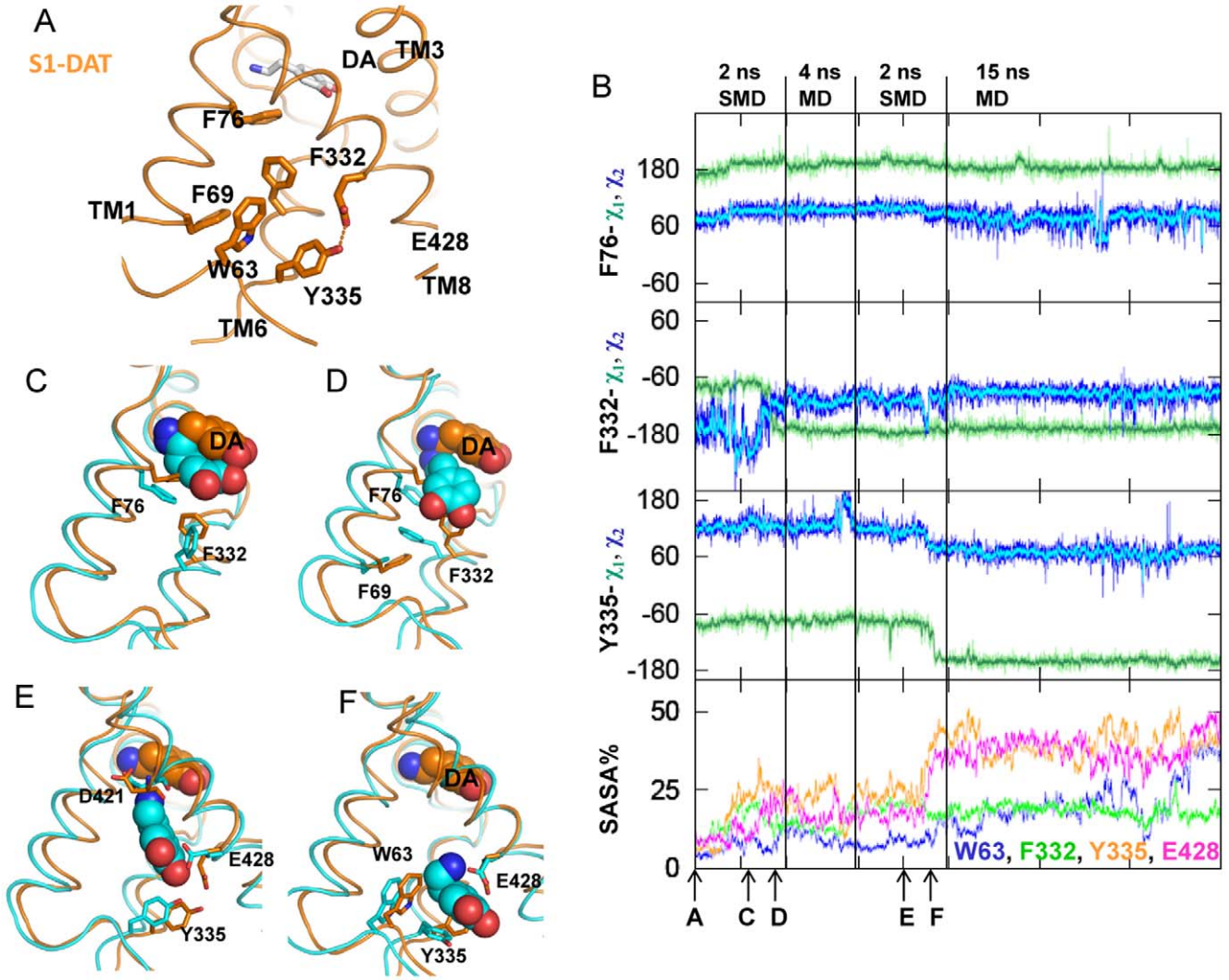

Figure 4. Conformational changes in the aromatic cluster during DA movement inward from the S1 site. (**A**) The cluster of aromatic residues from TMs 1 and 6 shown in S1-DAT is important for conformational transitions; DA in the S1 site is rendered in stick representation. Orange dashed line indicates H-bond of Y335$^{6.68}$ to E428$^{8.66}$. (**B**) Time evolution of dihedrals and SASA (bottom panel) during inward pulling in SMD and MD alternation. Time points marked by the A, B, C, D, E, F arrows on the x-axis correspond to the structures shown in the (**A**)–(**F**) panels. The lines in the SASA plot are coded in colors corresponding to the residues names in the same colors. (**C**) The change in the rotamer of F76$^{1.42}$ from the conformation in S1-DAT (orange) to the configuration at the time point indicated by the C arrow in (**B**) (cyan), which allows the downward movement of DA. (**D**) The subsequent change in the rotamer of F332$^{6.65}$ (same color coding as in (**C**)) as DA moves to the position originally occupied by the sidechain of F332$^{6.65}$. (**E**) When DA is slowly pulled down a bit further in the SMD protocol, its amine forms a new H-bond with the carboxyl oxygen of D421$^{8.59}$ which coordinates Na2 in S1-DAT, and its hydroxyl groups forms H-bonds with the sidechain carboxyl group of E428$^{8.66}$. Time is indicated by the E arrow in (**B**). (**F**) The rotamer of Y335$^{6.68}$ changes last, breaking the H-bond between Y335$^{6.68}$ and E428$^{8.66}$. DA moves to the position originally occupied by the sidechain of Y335$^{6.68}$ and E428$^{8.66}$. Time is indicated by the F arrow in (**B**).
doi:10.1371/journal.pone.0016350.g004

movement in TMs1b and 6a in the transition between S1-DAT and the inward-facing conformation. Interestingly, comparing LeuT structures in an occluded state [15] and in an outward-facing state [12], it is the intracellular segments TMs1a and 6b that were considered to remain immobile, while the extracellular TMs1b and 6a tilt outwards. The findings described here are also consistent with previously observed changes in the Tyt1 transporter upon opening of the translocation pathway, where this opening is associated with increased solvent accessibility of C18$^{1.39}$ and C238$^{6.65}$ [28]. The increased solvent accessibility at these two positions in Tyt1 was attributed to the rearrangement in TMs1a and 6b in the inward-facing conformation [28]. In the inward-facing conformation of DAT, TMs1a and 6b also move away from each other and the corresponding residues at the two positions, V73$^{1.39}$ (data not shown) and F332$^{6.65}$ (Dehnes et al, manuscript in prep), become more solvent accessible. These results, together with the corresponding observations in LeuT, support the view that TMs1 and 6 do not rock like a rigid bundle [21] when the transporter converts from the outward-facing to occluded conformation, and then to the inward-facing conformation (see Concluding Remarks). Indeed, the rearrangements of TMs1b-6a and TMs1a-6b appear to be driven by different local rearrangements and are thus separated during the transport cycle.

Other types of hinge regions comprise one or more conserved Gly/Pro/Thr/Ser/Cys residues (e.g., G55$^{2.48}$, P57$^{2.50}$, G294$^{7.45}$, G408$^{10.52}$ and P457$^{11.50}$) that enable rigid-body motions of helical segments. Using the Prokink analysis tool [59] implemented in the

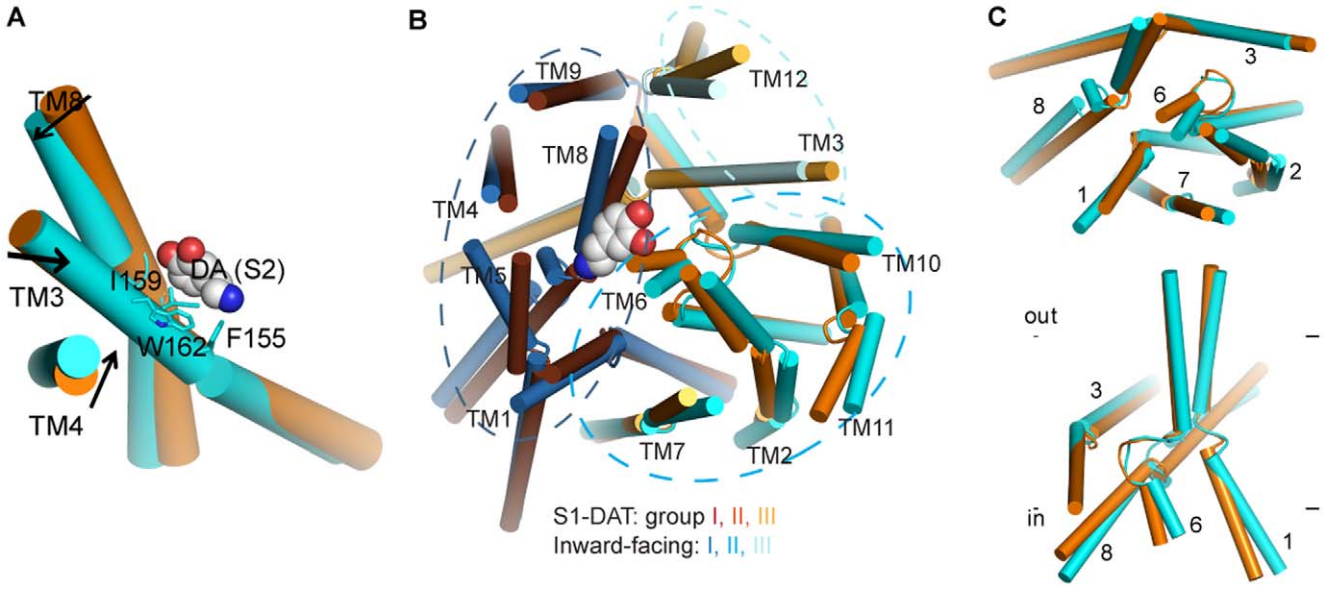

Figure 5. The global rearrangement from S1-DAT to the inward-facing conformation. (**A**) The global rearrangement of TMs3, 4 and 8 at the extracellular side, from S1-DAT (orange) to the inward-facing conformation (cyan). Proteins are aligned with RMSDTT [53] using the entire models. In the inward-facing conformation, TM3 residues F155$^{3.49}$, I159$^{3.53}$ and W162$^{3.56}$ (in sticks) are in direct contact with DA (in spheres, colored by atom type) in the S2 site. (**B**) Viewed from the intracellular side, the movement of the 12 intracellular TM segments (rendered in cartoon) can be partitioned into three groups as indicated by the dotted circles (see text). During the transition to the inward-facing conformation, the first group (colored in chocolate brown for S1-DAT and blue for the inward-facing conformation) moves outward; the second group (orange for S1-DAT and cyan for the inward-facing conformation) moves outward and away from the first group; the third group (yellow for S1-DAT and pale cyan for the inward-facing conformation) moves inward. DA is rendered in spheres and colored by atom types. (**C**) The global movement of selected TMs viewed from the intracellular side (top panel) and parallel to the membrane (bottom panel). During the transition, the extracellular ends of segments TM1b and TM6a do not move, while the intracellular end segments TMs1a and 6b swing away, non-symmetrically, from TMs 3 and 8 to open the substrate translocation pathway. TM1a moves substantially more, thereby distancing itself from TM6b.
doi:10.1371/journal.pone.0016350.g005

Simulaid suite [60] we found that for most TMs, the bend angle and face shift values produced by TM helix breakers change significantly in the transitions (Table 5). These local conformational changes connect individual TMs to the configuration changes propagated from the S2 to the S1 site, and further from the S1 site to the intracellular side of the transporter (see Text S2 and Figures S5, S6, S7 within File S2).

Experimental support for these observations was obtained from the rich structure-function information in the literature collected through the TRAC information management platform [57]. The results show that mutations of corresponding residues in these hinge regions in various NSS transporters disrupt the binding profile and/or the translocation cycle, as indicated by decreased binding affinities of substrates and ligands, increased K_m and/or decreased rates of transport, or altered DA efflux (see Table 5 and references therein). This underscores the functional importance of conformational changes associated with "hinges" in the course of the transition between functional states of the transporter.

Interaction networks are reconfigured in the transition. A series of previously identified interaction networks [16] that were viewed as "gates", were found here to participate in the conformational rearrangements underlying the state-to-state transitions by a mechanism of reconfiguration of interaction partners. Thus, networks stabilized by specific interactions such as salt bridges and H-bonds [16] need to be replaced by newly formed interactions to compensate for the energy loss. The intricacy of this reconfiguration suggests that modeling the global configurational changes based on global 3D folding-symmetry considerations cannot offer sufficient insight into the transitions. For example, we had shown that in S1-DAT the cation-pi interaction of Y335$^{6.68}$ with R60$^{1.25(NT)}$ stabilizes a salt bridge between R60$^{1.25(NT)}$ and D436$^{8.74}$, and that this intracellular interaction network regulates conformational transitions in DAT [16]. Here we reported that Y335$^{6.68}$ H-bonds to E428$^{8.66}$ in S1-DAT, but not in the inward-facing conformation (Figure 6) in which Y335$^{6.68}$ forms an H-bond with T62$^{1.27(NT)}$. The loss of the Y335$^{6.68}$ interaction with E428$^{8.66}$ destabilizes S1-DAT and steers the transporter towards an inward-facing conformation. The remodeling of this interaction network alters the capability of the transporter to alternate freely between S1-DAT and the inward-facing conformations that is seen to require a set of local rearrangements, rather than a purely symmetric rearrangement of TM segments.

Notably, the effect of Y335$^{6.68}$ mutation to Ala was shown to be rescuable by the addition of Zn^{2+} rescues [61], and the mechanism explained by the ability of Zn^{2+} to replace the energetically favorable Y335$^{6.68}$ interaction with R60$^{(NT)}$ thereby reinforcing S1-DAT, and restoring the equilibrium between S1-DAT and the inward-facing conformation that had been lost in the Y335$^{6.68}$A mutant [16]. Zn^{2+} binding to an endogenous site within the extracellular loops of the wild type (WT) DAT was shown to potently inhibit transport, while substrate binding can still take place [3,62]. Considering the reconfiguration of the interaction network we describe, the details of S1-DAT and the inward-facing conformation we observed provide an atomistic-level mechanism for these findings related to the nature of the endogenous binding site for Zn^{2+} that consists of residues H193^{EL2}, H375^{EL4a} and E396^{EL4b}. In S1-DAT, the average C_α distance between H375^{EL4a} and E396^{El4b} is 13 Å, suitable for Zn^{2+} binding [63] (Figure 7). In contrast, in the inward-facing conformation model this site is no

Table 5. ProKink analysis.

Residues	bend angle				face shift				References
	S1-DAT		inward-facing		S1-DAT		inward-facing		
	Avg.	std	Avg.	std	Avg.	std	Avg.	std	
L80$^{1.46}$	32.8	2.3	38.5	2.7	127.3	6.6	165.0	5.8	[77,78]
P101$^{2.39}$	12.0	3.9	19.4	3.1	26.8	13.1	9.9	11.1	[5–9]
P112$^{2.50}$	19.3	3.0	24.1	2.7	117.7	40.2	9.1	144.5	[5,6,9,79]
S149$^{3.43}$	22.0	2.8	14.5	2.7	13.3	6.1	13.7	6.3	[80]
G153$^{3.47}$	10.2	3.7	19.4	3.7	18.4	7.4	14.7	6.8	[80]
S254$^{4.61}$	43.2	2.8	55.0	3.4	10.0	10.5	41.8	8.9	[81–83]
T269$^{5.46}$	6.0	3.3	15.8	4.0	−13.5	5.4	15.7	7.0	[82,84]
P273$^{5.50}$	22.3	5.2	24.2	5.1	59.5	20.3	58.2	18.3	[5,6,84,85]
S354$^{7.39}$	6.2	2.2	6.0	2.6	8.0	6.8	12.1	5.5	[82,86–89]
S357$^{7.42}$	6.2	2.0	6.0	1.9	21.5	7.7	12.7	6.3	[82,88,90–92]
S422$^{8.60}$	14.9	3.1	14.2	3.1	0.1	8.6	44.3	9.4	[83,93]
G426$^{8.64}$	17.1	5.2	11.9	4.8	18.9	14.8	25.3	13.2	n/a
T456$^{9.49}$	6.2	2.7	7.1	2.8	32.1	7.4	26.8	8.0	[82,87]
S460$^{9.53}$	5.9	3.2	6.6	3.4	15.8	8.4	17.7	8.3	[82,94]
G481$^{10.53}$	31.6	2.4	36.6	2.2	59.2	8.4	57.6	16.3	n/a
S483$^{10.56}$	30.4	3.1	33.7	2.1	137.1	4.5	80.5	4.0	[82,95,96]

doi:10.1371/journal.pone.0016350.t005

longer suitable for Zn^{2+} binding because both EL2 and EL4b moved down toward S2, and EL4a moved away from EL4b so that the corresponding C_α distance increased to 15 Å. Accordingly, Zn^{2+} binding prefers the occluded conformation of WT DAT and by stabilizing it prevents the transition to the inward-open (facing) state, thus inhibiting translocation.

The detailed atomistic model of the allosteric mechanism that emerges from this study. Using SMD simulations with extended MD equilibrations we have identified detailed contributions of specific structural elements to the transition between states visited by the transporter molecule in the process of substrate translocation from the primary S1 binding site both to the extracellular and to the intracellular end of the protein. In the movement of substrate from S1 to the intracellular side, these structural elements perform an ordered sequence of local rearrangements that are triggered by the binding of substrate in the S2 site. This allosteric mechanism, identified here for DAT from the SMD simulations and extensive MD equilibrations of the resulting intermediate states, reconfigures a conserved spatial network of interactions (either direct, or through interposed substrate or water molecules) among residues in non-consecutive sequence loci, in a defined temporal sequence. Together, the local conformational changes revealed in the computational modeling of the process give rise to the global rearrangements of TM and

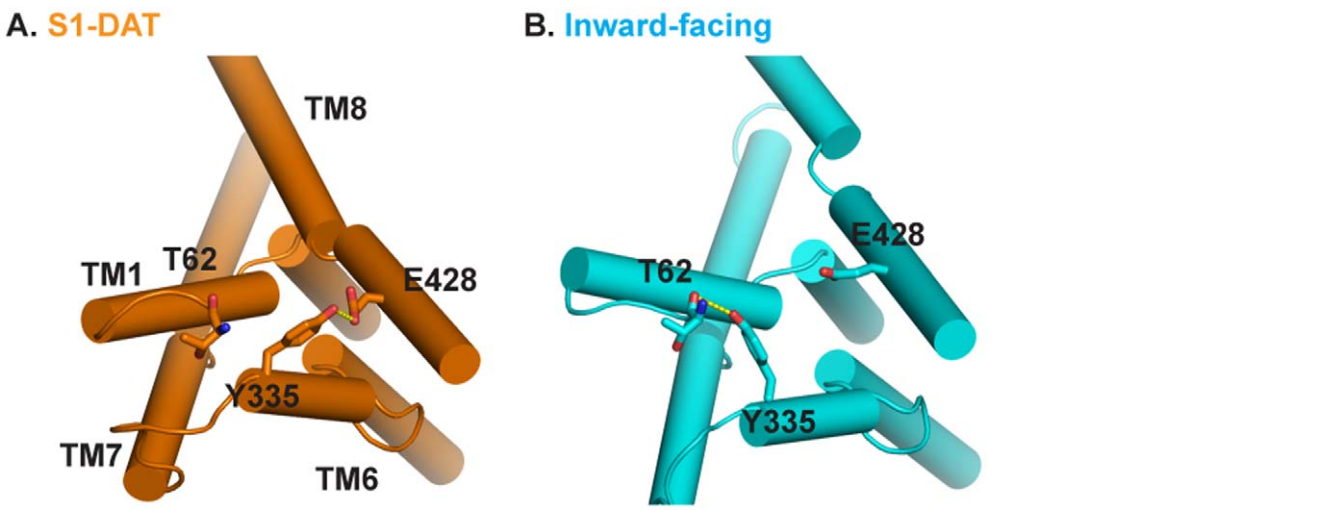

Figure 6. Changes in intracellular interaction networks. Y335$^{6.68}$ forms an H-bond with E428$^{8.66}$ in S1-DAT (**A**), and switches its H-bond partner to T62$^{1.27(NT)}$ in the inward-facing conformation (**B**).
doi:10.1371/journal.pone.0016350.g006

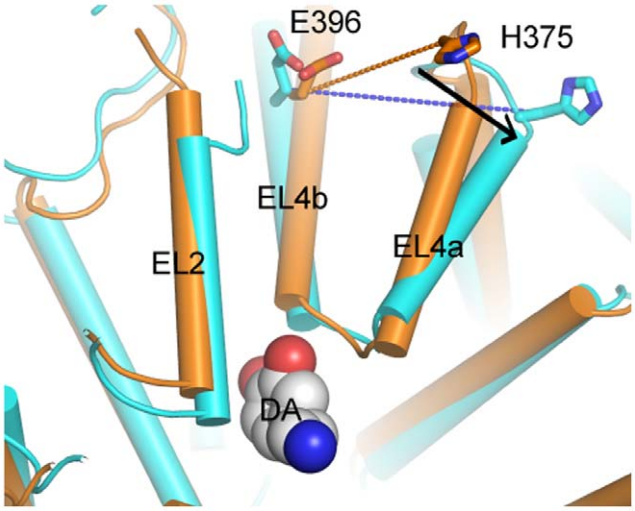

Figure 7. The endogenous Zn^{2+} binding site. Extracellular portions of DAT containing the endogenous Zn^{2+} binding site. S1-DAT (orange) and the inward-facing DAT (cyan) are aligned with RMSDTT using the whole structure and rendered in cartoon. The sidechains of Zn^{2+} binding residues $H375^{EL4a}$ and $E396^{EL4b}$ are rendered in sticks. In S1-DAT, the average C_α distance between $H375^{EL4a}$ and $E396^{EL4b}$ is 13 Å (orange dashed line). The distance increases to 15 Å in the inward-facing conformation (blue dashed line).
doi:10.1371/journal.pone.0016350.g007

loop segments that are captured in the types of conceptual models referring to the molecule undergoing transitions between states, e.g., from outward-open/facing to inward-open/facing states of the transporter.

The detailed atomistic model of the allosteric mechanism that emerges from this study achieves the same conformational endpoints as the classical alternating-access model for transport. However, the classical model is not structurally or mechanistically explicit. It invokes unspecified extracellular and intracellular gates alternating between open and close states without a defined connecting pathway, and would require the transporter molecule to traverse the underlying conformational states sequentially from outward-facing to S1-DAT and then to inward-facing [20,64–66]. Here, we describe for the first time for DAT the molecular details of a substrate movement mechanism in a manner that is directly amenable to experimental verification, as illustrated previously for LeuT [34,56].

The crystal structure of LeuT with a leucine and two Na^+ bound to the unwound regions of TMs1 and 6 suggested that these unwound regions are relatively flexible and thus may serve as hinges for the conformational transition [15]. Following the classical model, the intracellular TM segments 1a and 6b, and the corresponding extracellular segments 1b and 6a, were proposed to move in an alternating fashion relative to TMs3 and 8 [36]. Our results are in agreement with the identification of these segments as undergoing the most drastic rearrangements in the conformational transition (albeit not to the same extent). However, the nature of the conformational transition suggested by the dynamics revealed in this study is not compatible with simple rigid body movements, especially not for a bundle of TMs [21]. Thus, the allosteric mechanism triggered by the binding of substrate in the S2 site (Figure 8) in the presence of the two Na^+ and the substrate in the S1 site, which was observed from the atomistic simulations of the DAT structural model, suggests an ordered series of concerted conformational rearrangements in flexible regions that lead to the remodeling of interaction networks in a sequential manner. Specific hinge regions within the TMs (TMs2, 7, 10 and 11) enable the resulting large-scale segment rearrangements that characterize the resulting transition from the occluded to the inward-facing state. The dependence of the large conformational transitions and rearrangements on specific structural elements with identified mechanistic contributions suggests the possibility of various intermediate and functionally-specialized molecular conformations that can be adopted by individual members of the NSS family of transporter proteins.

Materials and Methods

Construction of function-related conformational states of DAT

DAT residue numbering. The DAT residue numbering scheme used here includes, in addition to the sequence-based numbering, a generic numbering system defined in [35,67]. According to this scheme, the most conserved residue in each TM is assigned a number 50, and then a pair of numbers (A1.A2) is used to identify each residue, where A1 refers to the TM number and A2 denotes the position of the amino acid relative to the most conserved residue in the TM (A2 numbers decrease from 50 towards the N-terminus and increase towards the C-terminus).

Homology modeling of DAT and construction of the simulation system. We had recently described results for a homology model of DAT and simulated it in explicit water and lipid environment [39]. The general protocol and the structure-based sequence alignment for homology modeling and ligand docking is as described there and earlier [35]. Briefly, the homology model uses as the template the known crystal structures for the cognate and homologous structure of LeuT [15]. DA was placed in the S1 site by aligning its amine group and hydrophobic portion with those of the structure leucine in the LeuT structure, and the long equilibration refines the interactions between DA and DAT. The two Na^+ ions were positioned equivalently to those in LeuT and a Cl^- ion was placed based on the chloride binding site described in [42]. The final model was immersed in an explicit water/lipid box to construct the simulated system.

Substrate movement towards the extracellular side. Constant velocity SMD simulations were used to explore the extracellular translocation pathway and the S2 site following a protocol described previously for a similar study of LeuT [29]. The SMD simulations were performed on an equilibrated DAT model with a substrate present in the S1 site [39]. A velocity of 4 Å/ns and a harmonic constant of 4 kcal/(mol·Å^2) were used in the pulling protocol of SMD for the substrate in the S1 site moving towards the extracellular side. As before, the force is applied through a connecting spring tethered at the center of mass of the ligand [29,68,69]. As described for the LeuT protocol, about 100 residues in the bottom parts of TMs 2, 4, 5, 7, 9, 10, 11 and 12 were constrained in the Z direction during the SMD. The entire simulation was performed in two phases. In Phase I, 2 ns of SMD simulation was followed by 4 ns of equilibration, while in Phase II 2 ns of SMD simulation was followed by 10 ns of equilibration. After 10 ns of equilibration a substrate was introduced again in the S1 site and the entire system with the two substrates (S1,S2-DAT) was equilibrated for 25 ns.

Substrate movement towards the cytoplasm. The SMD simulation was performed on the equilibrated S1,S2-DAT model to explore the intracellular translocation pathway and an inward-facing conformation. Step-wise decreased velocities of 10 Å/ns (for the first 200 ps), 5 Å/ns (for the subsequent 300 ps) and 2.5 Å/ns

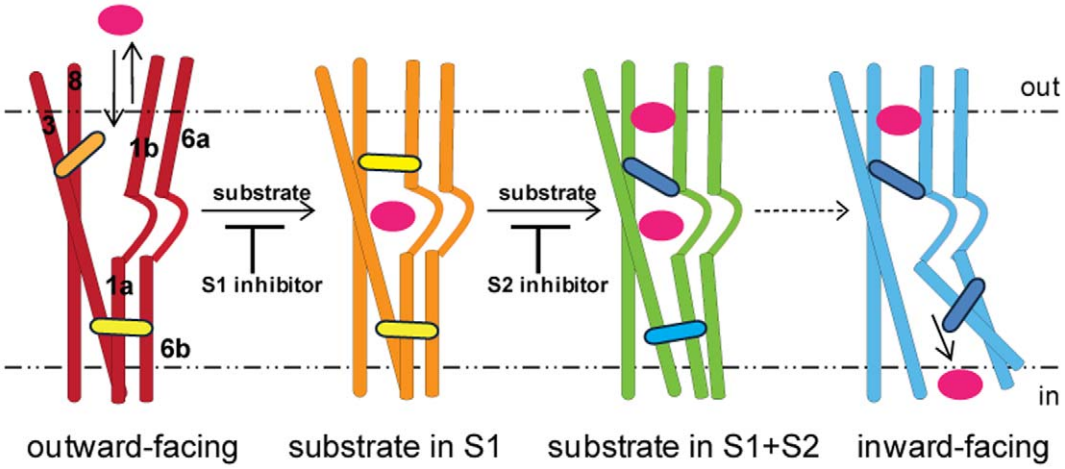

Figure 8. Cartoon model of a substrate translocation cycle for DAT. Substrate binding in the outward-facing model (red) promotes the formation of an occluded conformation (orange). The binding of a second substrate (doubly occupied state in green) induces conformational changes in the S1 site and the intracellular side through conserved interaction networks (colored lozenges) positioned between the S2 and S1 sites, which reorganize the interaction network at the intracellular end, eventually leading to the release of substrate in the S1 site from the inward-facing conformation (cyan). Inhibitors that bind to the S1 site block the formation of S1,S2-DAT and thus the translocation. Inhibitors that bind to the S2 site inhibit the release of S1 and act as translocation de-couplers [29].
doi:10.1371/journal.pone.0016350.g008

(for the last 1.5 ns) and a harmonic constant of 4 kcal/(mol·Å2) were used to move the substrate towards the cytoplasm in the established SMD protocol. About 100 residues in the upper part of TMs4, 5, 7, 9, 10, 11 and 12 were constrained in the Z direction during the SMD. Two parallel simulations were carried out to pull substrate from the S1 site to the intracellular side. The first simulation was performed in two phases. In Phase I, 2 ns of SMD simulation was followed by 4 ns of equilibration, while in Phase II 2 ns of SMD simulation was followed by 15 ns of equilibration. The second simulation was performed in three phases. In Phases I and II, 2 ns of SMD simulation was followed by 4 ns of equilibration, while in Phase III 2 ns of SMD simulation was followed by 15 ns of equilibration.

Residues in the S1 and S2 sites. Residues were identified as part of the S1 site if during the dynamics simulations they are within 3.5 Å of the substrate at the S1 site for more than 5% of the time during equilibration of either S1-DATor S1,S2-DAT. Residues were treated as part of the S2 site if they are within 3.5 Å of the substrate at the S2 site for more than 5% of the time during equilibration of either S1,S2-DAT or the inward-facing model. For the analysis, the first 5 ns trajectories were discarded. Snapshots were extracted every 10 ps.

Identifying residues in the transport pathway. Simulations moving the substrate towards the extracellular space in the single substrate model were used to identify residues in the transport pathway from the extracellular side to the S1 site of DAT. Residues within 3.5 Å of the substrate were identified at every 2 ps during SMD and at every 5 ps during the equilibration. A complete list of residues that remained in contact with the substrate as it moved from the S1 site towards the extracellular side was prepared for DAT. For every residue in the complete list the time point when a given residue first made contact with the substrate and when it was last in contact with the substrate was recorded for each individual SMD and MD trajectories. For every residue in the list, the percentage of time for which the given residue remained in contact with the substrate between its first and last contact time point was calculated. The residues that remained in contact with the substrate for more than 5% of the time in any individual trajectory were classified as belonging to the extracellular transport pathway. Similarly, simulations of S1,S2-DAT that pulled the substrate towards the cytoplasm were used for identifying the residues in the transport pathway from the S1 site to the cytoplasm of DAT. Residues in either the S1 or S2 site were excluded from transport pathways.

Structural Analysis

Number of waters in DAT along the transport pathway. The internal water pathway in DAT was monitored from the average numbers of water molecules in the pathway along the Z coordinate (the membrane normal) every 50 ps for the last 1 ns of various equilibration trajectories of DAT: S1-DAT, S1,S2-DAT and the inward-facing conformation. All trajectories were aligned to a reference (S1-DAT) before counting.

Substrate-water interaction energies. The interaction energies were calculated with the CHARMM27 force field [70] using NAMD [71]. All the water molecules were treated as one group and DA as the other.

Calculation of dihedral angles. Dihedral angles ($\chi1$, $\chi2$) in the rotamers of residues $F76^{1.42}$, $F332^{6.65}$ and $Y335^{6.68}$ were calculated with ptraj in AMBER9 [72] every 5 ps for the 25 ns equilibration trajectory of the S1,S2-DAT. Similarly, dihedral angles ($\chi1$, $\chi2$) and φ, ψ angles of residues $W63^{1.29}$, $F69^{1.35}$, $F76^{1.42}$, $F332^{6.65}$, $Y335^{6.68}$ and $E428^{8.66}$ were calculated for the final 2 ns equilibration trajectories of S1-DAT, inward-facing and S1,S2-DAT models.

Calculation of Solvent accessibility surface area (SASA). For $W63^{1.29}$, $F69^{1.35}$, $F76^{1.42}$, $F332^{6.65}$, $Y335^{6.68}$ and $E428^{8.66}$ values were calculated from the 25 ns S1,S2-DAT equilibration trajectory and the two intracellular pulling trajectories. SASA was recorded every 5 ps for the equilibration trajectories and every 2 ps for the SMD trajectories. Only surface area accessible to solvent was counted; surface area exposed to lipids was treated as buried. SASA percentage was obtained by dividing the SASA value for residue X by a reference value calculated for X in a Gly-X-Gly tripeptide in extended conformation [73].

Calculation of helix kink parameters. To describe local distortions in TMs during the MD simulation caused by proline or consecutive glycine [74] as well as other helix-disrupting residues

serine, threonine and cysteine [50], we calculated bend and face shift angles around the following residues: $L80^{1.46}$, $P101^{2.39}$, $Pro112^{2.50}$, $S149^{3.43}$, $G153^{3.47}$, $S254^{4.61}$, $T269^{5.46}$, $S354^{7.39}$, $S357^{7.42}$, $S422^{8.60}$, $G426^{8.64}$, $T456^{9.49}$, $G481^{10.53}$ and $S483^{10.56}$. Calculation was also carried out for $Leu80^{1.46}$ to quantify the changes in TM1a and TM1b since $L80^{1.46}$ is located in the unwound region between TM1a and TM1b. The bend angle, which measures the extent of helical kink, is defined as the angle between pre-kink and post-kink parts in a TM, and the face shift angle describes the distortion that causes a helix to twist in such a way that amino acids previously facing the same side of the helix are now shifted and positioned on different sides of the TM [59].

To quantify the changes in the helix distortion parameters throughout the MD trajectory, we used the ProKink package [59] in the publicly available software Simulaid [60]. Details about the geometric definitions and the computational protocol implemented in ProKink can be found in [59]. In short, DAT snapshots at different time-points were fitted onto the starting reference structure of the protein, and the C_α atom of the Pro or other helix-disrupting residue in the relevant TM was positioned at the Cartesian origin. To calculate the bend angle of a helix, the coordinate system was rotated for each trajectory frame around the axis passing through the pre-proline helical segment until the long axes of the post and pre-proline parts were in the same plane. From this orientation, the bend or kink angle was measured as the angle between the axes of the two parts of the helix. To obtain the face shift angle, for each snapshot the post-proline segment, which included the Pro C_α atom was rotated so that both pre and post-proline helical parts shared a long axis [59]. The face shift angle was then calculated as the angle between projections of two vectors onto the plane perpendicular to the long axis: these vectors are the on connecting the Pro C_α atom with the Cartesian origin, and the average vector connecting the C_α atoms of the (i-3) and (i-4) amino acids with the origin.

Aligning different conformational states with RMSDTT to define global movements. Inward-facing conformations were aligned to occluded conformations for both DAT and LeuT using the plugin RMSDTT [53] of the VMD (Visual Molecular Dynamics) [75] program. The iterative fitting implemented in the RMSDTT plugin performs a by-residue weighted pairwise fitting, such that after each iteration, residues with lower average RMSD are assigned higher weights in the next iteration. A similar idea for improving the quality of the commonly used RMSD comparison had been described independently by Damm and Carlson [76]. In total, three iterations of fitting were carried out with default fitting parameters. The reported residue-based RMSD was calculated with RMSDTT when aligning the whole structure.

For additional methods, see Text S1 in File S1.

Supporting Information

File S1 Supplementary Methods details, figures, and tables detailing structural rearrangements in the different conformational states of DAT.
(DOC)

File S2 Hinge regions underlying the global and local conformational rearrangements in DAT and the hinge regions enabling these changes.
(DOC)

Acknowledgments

Computational support was provided by the National Science Foundation Terascale Computing System at the Texas Advanced Computing Center (TG-MCB090022 and TG-MCB080118N) and the computer facilities at the Institute of Computational Biomedicine of Weill Cornell Medical College.

Author Contributions

Conceived and designed the experiments: JAJ LS HW. Performed the experiments: JS. Analyzed the data: JS LS HW. Wrote the paper: JS JAJ LS HW.

References

1. Sonders MS, Quick M, Javitch JA (2005) How did the neurotransmitter cross the bilayer? A closer view. Curr Opin Neurobiol 15: 296–304.
2. Javitch JA (1998) Probing structure of neurotransmitter transporters by substituted-cysteine accessibility method. Methods Enzymol 296: 331–346.
3. Loland CJ, Norregaard L, Gether U (1999) Defining proximity relationships in the tertiary structure of the dopamine transporter. Identification of a conserved glutamic acid as a third coordinate in the endogenous Zn^{2+}-binding site. J Biol Chem 274: 36928–36934.
4. Norregaard L, Loland CJ, Gether U (2003) Evidence for distinct sodium-, dopamine-, and cocaine-dependent conformational changes in transmembrane segments 7 and 8 of the dopamine transporter. J Biol Chem 278: 30587–30596.
5. Lin Z, Itokawa M, Uhl GR (2000) Dopamine transporter proline mutations influence dopamine uptake, cocaine analog recognition, and expression. FASEB J 14: 715–728.
6. Itokawa M, Lin Z, Uhl GR (2002) Dopamine efflux via wild-type and mutant dopamine transporters: alanine substitution for proline-572 enhances efflux and reduces dependence on extracellular dopamine, sodium and chloride concentrations. Brain Res Mol Brain Res 108: 71–80.
7. Sen N, Shi L, Beuming T, Weinstein H, Javitch JA (2005) A pincer-like configuration of TM2 in the human dopamine transporter is responsible for indirect effects on cocaine binding. Neuropharmacology 49: 780–790.
8. Lin Z, Uhl GR (2005) Proline mutations induce negative-dosage effects on uptake velocity of the dopamine transporter. J Neurochem 94: 276–287.
9. Sucic S, Bryan-Lluka LJ (2005) Roles of transmembrane domain 2 and the first intracellular loop in human noradrenaline transporter function: pharmacological and SCAM analysis. J Neurochem 94: 1620–1630.
10. Quick M, Winther AM, Shi L, Nissen P, Weinstein H, et al. (2009) Binding of an octylglucoside detergent molecule in the second substrate (S2) site of LeuT establishes an inhibitor-bound conformation. Proc Natl Acad Sci U S A 106: 5563–5568.
11. Singh SK, Yamashita A, Gouaux E (2007) Antidepressant binding site in a bacterial homologue of neurotransmitter transporters. Nature 448: 952–956.
12. Singh SK, Piscitelli CL, Yamashita A, Gouaux E (2008) A Competitive Inhibitor Traps LeuT in an Open-to-Out Conformation. Science 322: 1655–1661.
13. Zhou Z, Zhen J, Karpowich NK, Law CJ, Reith ME, et al. (2009) Antidepressant specificity of serotonin transporter suggested by three LeuT-SSRI structures. Nat Struct Mol Biol 16: 652–657.
14. Zhou Z, Zhen J, Karpowich NK, Goetz RM, Law CJ, et al. (2007) LeuT-desipramine structure reveals how antidepressants block neurotransmitter reuptake. Science 317: 1390–1393.
15. Yamashita A, Singh SK, Kawate T, Yan Jin Y, Gouaux E (2005) Crystal structure of a bacterial homologue of Na^+/Cl^- dependent neurotransmitter transporters. Nature 437: 215–223.
16. Kniazeff J, Shi L, Loland CJ, Javitch JA, Weinstein H, et al. (2008) An intracellular interaction network regulates conformational transitions in the dopamine transporter. J Biol Chem 283: 17691–17701.
17. Abramson J, Wright EM (2009) Structure and function of Na(+)-symporters with inverted repeats. Curr Opin Struct Biol 19: 425–432.
18. Gouaux E (2009) Review. The molecular logic of sodium-coupled neurotransmitter transporters. Philos Trans R Soc Lond B Biol Sci 364: 149–154.
19. Lolkema JS, Slotboom DJ (2008) The major amino acid transporter superfamily has a similar core structure as Na+-galactose and Na+-leucine transporters. Mol Membr Biol 25: 567–570.
20. Jardetzky O (1966) Simple Allosteric Model for Membrane Pumps. Nature 211: 969–970.
21. Forrest LR, Rudnick G (2009) The rocking bundle: a mechanism for ion-coupled solute flux by symmetrical transporters. Physiology (Bethesda) 24: 377–386.
22. Forrest LR, Tavoulari S, Zhang YW, Rudnick G, Honig B (2007) Identification of a chloride ion binding site in Na+/Cl -dependent transporters. Proc Natl Acad Sci U S A 104: 12761–12766.
23. Beuming T, Kniazeff J, Bergmann ML, Shi L, Gracia L, et al. (2008) The binding sites for cocaine and dopamine in the dopamine transporter overlap. Nat Neurosci 11: 780–789.

24. Crisman TJ, Qu S, Kanner BI, Forrest LR (2009) Inward-facing conformation of glutamate transporters as revealed by their inverted-topology structural repeats. Proc Natl Acad Sci U S A 106: 20752–20757.
25. Enkavi G, Tajkhorshid E (2010) Simulation of spontaneous substrate binding revealing the binding pathway and mechanism and initial conformational response of GlpT. Biochemistry 49: 1105–1114.
26. Khalili-Araghi F, Gumbart J, Wen PC, Sotomayor M, Tajkhorshid E, et al. (2009) Molecular dynamics simulations of membrane channels and transporters. Curr Opin Struct Biol 19: 128–137.
27. Li J, Tajkhorshid E (2009) Ion-releasing state of a secondary membrane transporter. Biophys J 97: L29–31.
28. Quick M, Yano H, Goldberg NR, Duan L, Beuming T, et al. (2006) State-dependent conformations of the translocation pathway in the tyrosine transporter Tyt1, a novel neurotransmitter:sodium symporter from Fusobacterium nucleatum. J Biol Chem 281: 26444–26454.
29. Shi L, Quick M, Zhao Y, Weinstein H, Javitch JA (2008) The mechanism of a neurotransmitter:sodium symporter–inward release of Na+ and substrate is triggered by substrate in a second binding site. Mol Cell 30: 667–677.
30. Zhao Y, Quick M, Shi L, Mehler EL, Weinstein H, et al. (2010) Substrate-dependent proton antiport in neurotransmitter:sodium symporters. Nat Chem Biol 6: 109–116.
31. Noskov SY, Roux B (2008) Control of Ion Selectivity in LeuT: Two Na+ Binding Sites with Two Different Mechanisms. Journal of Molecular Biology 377: 804–818.
32. Noskov SY (2008) Molecular mechanism of substrate specificity in the bacterial neutral amino acid transporter LeuT. Proteins: Structure, Function, and Bioinformatics 73: 851–863.
33. Shi L, Weinstein H (2010) Conformational rearrangements to the intracellular open states of the LeuT and ApcT transporters are modulated by common mechanisms. Biophys J 99: L103–105.
34. Zhao Y, Terry D, Shi L, Weinstein H, Blanchard SC, et al. (2010) Single-molecule dynamics of gating in a neurotransmitter transporter homologue. Nature 465: 188–193.
35. Beuming T, Shi L, Javitch JA, Weinstein H (2006) A comprehensive structure-based alignment of prokaryotic and eukaryotic neurotransmitter/Na+ symporters (NSS) aids in the use of the LeuT structure to probe NSS structure and function. Mol Pharmacol 70: 1630–1642.
36. Krishnamurthy H, Piscitelli CL, Gouaux E (2009) Unlocking the molecular secrets of sodium-coupled transporters. Nature 459: 347–355.
37. Huang X, Zhan C-G (2007) How Dopamine Transporter Interacts with Dopamine: Insights from Molecular Modeling and Simulation. Biophys J 93: 3627–3639.
38. Patrick CG, Martín I, Christopher KS, Jeffry DM (2010) Molecular dynamics of leucine and dopamine transporter proteins in a model cell membrane lipid bilayer. Proteins: Structure, Function, and Bioinformatics 78: 797–811.
39. Guptaroy B, Zhang M, Bowton E, Binda F, Shi L, et al. (2009) A juxtamembrane mutation in the N terminus of the dopamine transporter induces preference for an inward-facing conformation. Mol Pharmacol 75: 514–524.
40. Celik L, Schiøtt B, Tajkhorshid E (2008) Substrate Binding and Formation of an Occluded State in the Leucine Transporter. Biophys J 94: 1600–1612.
41. Gu Y, Shrivastava IH, Amara SG, Bahar I (2009) Molecular simulations elucidate the substrate translocation pathway in a glutamate transporter. Proc Natl Acad Sci U S A 106: 2589–2594.
42. Zomot E, Bendahan A, Quick M, Zhao Y, Javitch JA, et al. (2007) Mechanism of chloride interaction with neurotransmitter:sodium symporters. Nature 449: 726–730.
43. Indarte M, Madura JD, Surratt CK (2008) Dopamine transporter comparative molecular modeling and binding site prediction using the $LeuT_{Aa}$ leucine transporter as a template. Proteins: Structure, Function, and Bioinformatics 70: 1033–1046.
44. Loland CJ, Granas C, Javitch JA, Gether U (2004) Identification of intracellular residues in the dopamine transporter critical for regulation of transporter conformation and cocaine binding. J Biol Chem 279: 3228–3238.
45. Ben-Yona A, Kanner BI (2009) Transmembrane domain 8 of the gamma-aminobutyric acid transporter GAT-1 lines a cytoplasmic accessibility pathway into its binding pocket. J Biol Chem 284: 9727–9732.
46. Suel GM, Lockless SW, Wall MA, Ranganathan R (2003) Evolutionarily conserved networks of residues mediate allosteric communication in proteins. Nat Struct Mol Biol 10: 59–69.
47. Ota N, Agard DA (2005) Intramolecular Signaling Pathways Revealed by Modeling Anisotropic Thermal Diffusion. Journal of Molecular Biology 351: 345–354.
48. Lockless SW, Ranganathan R (1999) Evolutionarily Conserved Pathways of Energetic Connectivity in Protein Families. Science 286: 295–299.
49. Crawley MJ (2007) The R book.John Wiley & Sons, Ltd. Chichester: West Sussex PO19 8SQ, England.
50. Visiers I, Ballesteros JA, Weinstein H (2002) Three-dimensional representations of G protein-coupled receptor structures and mechanisms. Methods Enzymol 343: 329–371.
51. Shi L, Liapakis G, Xu R, Guarnieri F, Ballesteros JA, et al. (2002) Beta2 adrenergic receptor activation. Modulation of the proline kink in transmembrane 6 by a rotamer toggle switch. J Biol Chem 277: 40989–40996.
52. Singh R, Hurst DP, Barnett-Norris J, Lynch DL, Reggio PH, et al. (2002) Activation of the cannabinoid CB1 receptor may involve a W6.48/F3.36 rotamer toggle switch. The Journal of Peptide Research 60: 357–370.
53. Gracia L (2005) RMSDTT: RMSD Trajectory Tool. 2.5 ed. Weill Medical College of Cornell University, Department of Physiology and Biophysics.
54. Russell RB, Barton GJ (1992) Multiple protein sequence alignment from tertiary structure comparison: assignment of global and residue confidence levels. Proteins 14: 309–323.
55. Eargle J, Wright D, Luthey-Schulten Z (2006) Multiple Alignment of protein structures and sequences for VMD. Bioinformatics 22: 504–506.
56. Claxton DP, Quick M, Shi L, de Carvalho FD, Weinstein H, et al. (2010) Ion/substrate-dependent conformational dynamics of a bacterial homolog of neurotransmitter:sodium symporters. Nat Struct Mol Biol 17: 822–829.
57. Shi L, Srdanovic M, Beuming T, Skrabanek L, Javitch JA, et al. (2010) TRAC — a platform for structure-function studies of NSS-proteins integrates information from bioinformatics and biomedical literature. Philadelphia, PA: 10th IEEE International Conference on Bioinformatics & Bioengineering.
58. Szilagyi A, Zavodszky P (2000) Structural differences between mesophilic, moderately thermophilic and extremely thermophilic protein subunits: results of a comprehensive survey. Structure 8: 493–504.
59. Visiers I, Braunheim BB, Weinstein H (2000) Prokink: a protocol for numerical evaluation of helix distortions by proline. Protein Eng 13: 603–606.
60. Mezei M (2010) Simulaid: A simulation facilitator and analysis program. J Comput Chem 31: 2658–2668.
61. Loland CJ, Norregaard L, Litman T, Gether U (2002) Generation of an activating Zn^{2+} switch in the dopamine transporter: mutation of an intracellular tyrosine constitutively alters the conformational equilibrium of the transport cycle. Proc Natl Acad Sci U S A 99: 1683–1688.
62. Norregaard L, Visiers I, Loland CJ, Ballesteros J, Weinstein H, et al. (2000) Structural probing of a microdomain in the dopamine transporter by engineering of artificial Zn2+ binding sites. Biochemistry 39: 15836–15846.
63. Elling CE, Thirstrup K, Nielsen SM, Hjorth SA, Schwartz TW (1997) Engineering of metal-ion sites as distance constraints in structural and functional analysis of 7TM receptors. Folding and Design 2: S76–S80.
64. Rudnick G (1998) Bioenergetics of neurotransmitter transport. J Bioenerg Biomembr 30: 173–185.
65. Abramson J, Smirnova I, Kasho V, Verner G, Kaback HR, et al. (2003) Structure and Mechanism of the Lactose Permease of Escherichia coli. Science 301: 610–615.
66. Yernool D, Boudker O, Jin Y, Gouaux E (2004) Structure of a glutamate transporter homologue from Pyrococcus horikoshii. Nature 431: 811–818.
67. Goldberg NR, Beuming T, Soyer OS, Goldstein RA, Weinstein H, et al. (2003) Probing conformational changes in neurotransmitter transporters: a structural context. European Journal of Pharmacology 479: 3–12.
68. Isralewitz B, Gao M, Schulten K (2001) Steered molecular dynamics and mechanical functions of proteins. Curr Opin Struct Biol 11: 224–230.
69. Jensen MO, Yin Y, Tajkhorshid E, Schulten K (2007) Sugar transport across lactose permease probed by steered molecular dynamics. Biophys J 93: 92–102.
70. MacKerellJr AD, Banavali N, Foloppe N (2000) Development and current status of the CHARMM force field for nucleic acids. Biopolymers 56: 257–265.
71. Phillips JC, Braun R, Wang W, Gumbart J, Tajkhorshid E, et al. (2005) Scalable molecular dynamics with NAMD. J Comput Chem 26: 1781–1802.
72. Case DA, Darden TA, Cheatham III TE, Simmerling CL, Wang J, et al. (2006) AMBER 9. University of California, San Francisco.
73. Miller S, Lesk AM, Janin J, Chothia C (1987) The accessible surface area and stability of oligomeric proteins. Nature 328: 834–836.
74. Sansom MS, Weinstein H (2000) Hinges, swivels and switches: the role of prolines in signalling via transmembrane alpha-helices. Trends Pharmacol Sci 21: 445–451.
75. Humphrey W, Dalke A, Schulten K (1996) VMD: visual molecular dynamics. J Mol Graph 14: 33–38.
76. Damm KL, Carlson HA (2006) Gaussian-weighted RMSD superposition of proteins: a structural comparison for flexible proteins and predicted protein structures. Biophys J 90: 4558–4573.
77. Henry LK, Adkins EM, Han Q, Blakely RD (2003) Serotonin and cocaine-sensitive inactivation of human serotonin transporters by methanethiosulfonates targeted to transmembrane domain I. J Biol Chem 278: 37052–37063.
78. Zhou Y, Bennett ER, Kanner BI (2004) The aqueous accessibility in the external half of transmembrane domain I of the GABA transporter GAT-1 Is modulated by its ligands. J Biol Chem 279: 13800–13808.
79. Sato Y, Zhang YW, Androutsellis-Theotokis A, Rudnick G (2004) Analysis of transmembrane domain 2 of rat serotonin transporter by cysteine scanning mutagenesis. J Biol Chem 279: 22926–22933.
80. Dodd JR, Christie DL (2005) Substituted cysteine accessibility of the third transmembrane domain of the creatine transporter: defining a transport pathway. J Biol Chem 280: 32649–32654.
81. Golovanevsky V, Kanner BI (1999) The reactivity of the gamma-aminobutyric acid transporter GAT-1 toward sulfhydryl reagents is conformationally sensitive. Identification of a major target residue. J Biol Chem 274: 23020–23026.
82. Itokawa M, Lin Z, Cai NS, Wu C, Kitayama S, et al. (2000) Dopamine transporter transmembrane domain polar mutants: ΔG and $\Delta\Delta G$ values implicate regions important for transporter functions. Mol Pharmacol 57: 1093–1103.

83. Lin Z, Zhang PW, Zhu X, Melgari JM, Huff R, et al. (2003) Phosphatidylinositol 3-kinase, protein kinase C, and MEK1/2 kinase regulation of dopamine transporters (DAT) require N-terminal DAT phosphoacceptor sites. J Biol Chem 278: 20162–20170.
84. Zhang YW, Rudnick G (2005) Cysteine-scanning mutagenesis of serotonin transporter intracellular loop 2 suggests an alpha-helical conformation. J Biol Chem 280: 30807–30813.
85. Paczkowski FA, Bryan-Lluka LJ (2004) Role of proline residues in the expression and function of the human noradrenaline transporter. J Neurochem 88: 203–211.
86. Kitayama S, Wang JB, Uhl GR (1993) Dopamine transporter mutants selectively enhance MPP+ transport. Synapse 15: 58–62.
87. Sur C, Schloss P, Betz H (1997) The rat serotonin transporter: identification of cysteine residues important for substrate transport. Biochem Biophys Res Commun 241: 68–72.
88. Penado KM, Rudnick G, Stephan MM (1998) Critical amino acid residues in transmembrane span 7 of the serotonin transporter identified by random mutagenesis. J Biol Chem 273: 28098–28106.
89. Kamdar G, Penado KM, Rudnick G, Stephan MM (2001) Functional role of critical stripe residues in transmembrane span 7 of the serotonin transporter. Effects of Na+, Li+, and methanethiosulfonate reagents. J Biol Chem 276: 4038–4045.
90. Kitayama S, Shimada S, Xu H, Markham L, Donovan DM, et al. (1992) Dopamine transporter site-directed mutations differentially alter substrate transport and cocaine binding. Proc Natl Acad Sci U S A 89: 7782–7785.
91. Danek Burgess KS, Justice JB, Jr. (1999) Effects of serine mutations in transmembrane domain 7 of the human norepinephrine transporter on substrate binding and transport. J Neurochem 73: 656–664.
92. Dar DE, Mayo C, Uhl GR (2005) The interaction of methylphenidate and benztropine with the dopamine transporter is different than other substrates and ligands. Biochem Pharmacol 70: 461–469.
93. Zhou Y, Zomot E, Kanner BI (2006) Identification of a lithium interaction site in the gamma-aminobutyric acid (GABA) transporter GAT-1. J Biol Chem 281: 22092–22099.
94. Paczkowski FA, Bonisch H, Bryan-Lluka LJ (2002) Pharmacological properties of the naturally occurring Ala(457)Pro variant of the human norepinephrine transporter. Pharmacogenetics 12: 165–173.
95. Keller2nd PC, Stephan M, Glomska H, Rudnick G (2004) Cysteine-scanning mutagenesis of the fifth external loop of serotonin transporter. Biochemistry 43: 8510–8516.
96. Plenge P, Wiborg O (2005) High- and low-affinity binding of S-citalopram to the human serotonin transporter mutated at 20 putatively important amino acid positions. Neurosci Lett 383: 203–208.

The Substrate-driven Transition to an Inward-facing Conformation in the Functional Mechanism of the Dopamine Transporter

Jufang Shan, Jonathan A Javitch, Lei Shi and Harel Weinstein

Figure S1. Conformational changes in S1,S2-DAT compared to S1-DAT.

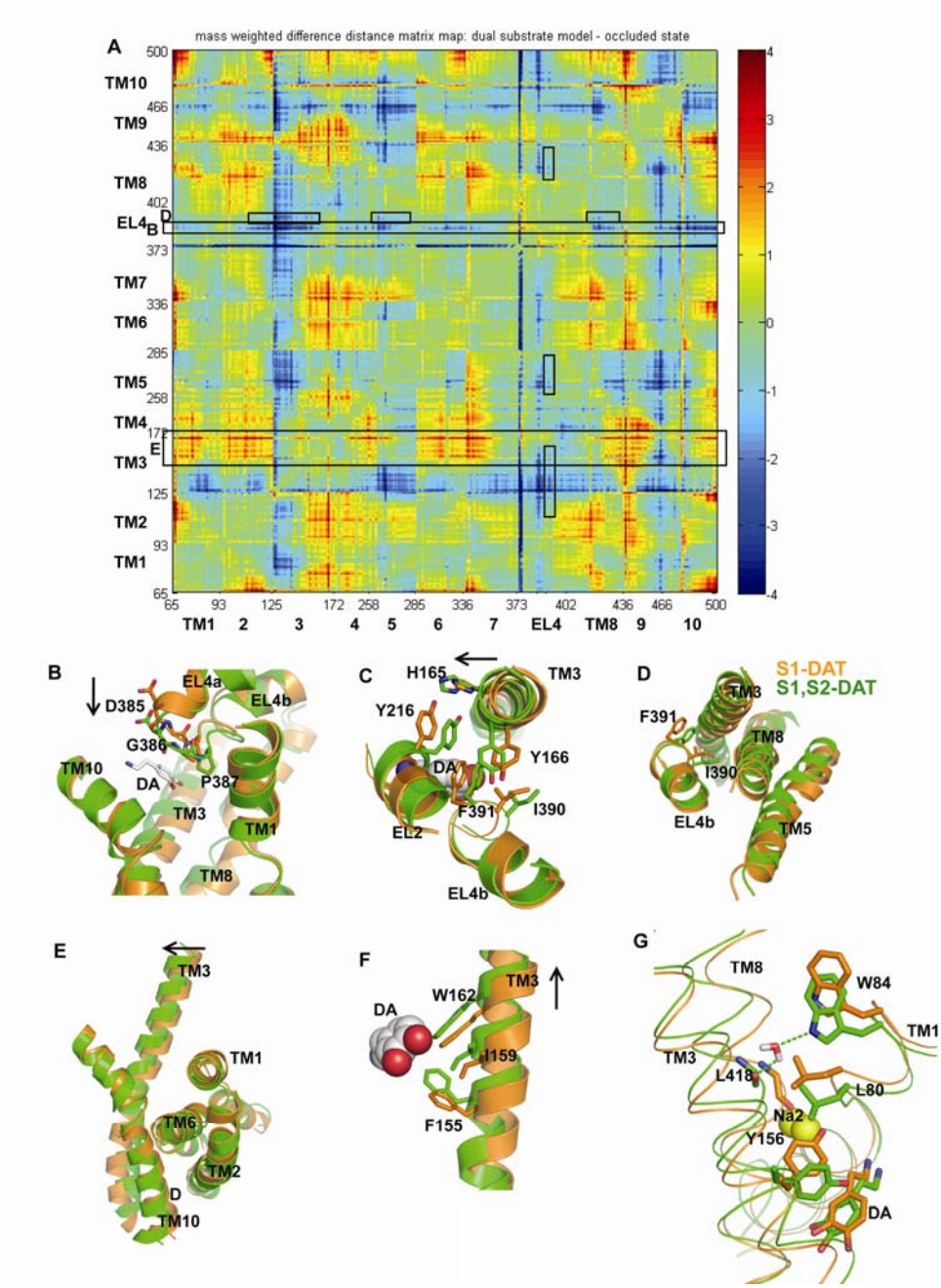

(**A**) The mass-weighted average difference distance matrix map (DDMP) for TM1 to TM10 and EL4 of S1,S2-DAT and S1-DAT. The distance matrices for S1-DAT and for S1,S2-DAT were calculated with ptraj [1], and then the S1-DAT matrix was subtracted from the S1,S2-DAT resulting in the DDMP. The DDMP was plotted with Matlab 2007b (The MathWorks Inc.) and colored by difference distance as shown in the color bar: distance changes > 4 Å are in red, equal to 0 Å in green, and < -4 Å, in blue. Positive change values indicate residues that moved away from each other when S1-DAT transitioned to S1,S2-DAT; negative changes mean that residues moved closer to each other in the transition; zero changes indicate that residues either didn't move or moved together in the same direction.

(**B**) $D385^{EL4}$, $G386^{EL4}$ and $P387^{EL4}$ moved downwards as the distances between them, and the intracellular segment of TM1 to TM10 in S1,S2-DAT, became smaller (highlighted in Figure S1A).

(**C**) When moving down, EL2 and EL4 pushed the extracellular segment of TM3 inwards to the S2 site through interactions between $Y216^{EL2}$, $I390^{EL4}$ and $F391^{EL4}$ on the two loops, and $H165^{3.59}$ and $Y166^{3.60}$ on TM3.

(**D**) In S1,S2-DAT, residues $I390^{EL4}$ and $F391^{EL4}$ moved closer to TMs3, 5 and the middle part of TM8.

(**E**) The extracellular segment of TM3 moved inward and away from several TMs including those that are opposite to TM3: TMs1a, 2, 6 and the extracellular segment of TM10.

(**F**) TM3 shifted up slightly along its helix axis and three residues: $F155^{3.49}$, $I159^{3.53}$ and $W162^{3.56}$ were positioned for interaction with S2.

(**G**) In the S1,S2-DAT, $L418^{8.56}$ flips its carbonyl group to interact through a water molecule with the downward moved $W84^{1.50}$. The middle portion of TM8 moves away from TM1. In S1-DAT, $L418^{8.56}$ coordinates with Na2. Colors are the same as in Figure 3. Helices are represented in cartoon, residues are in sticks and DA is either in sticks (**B**) or spheres (**C**, **F**).

Figure S2. SASA for the aromatic cluster residues during equilibration of S1,S2-DAT.

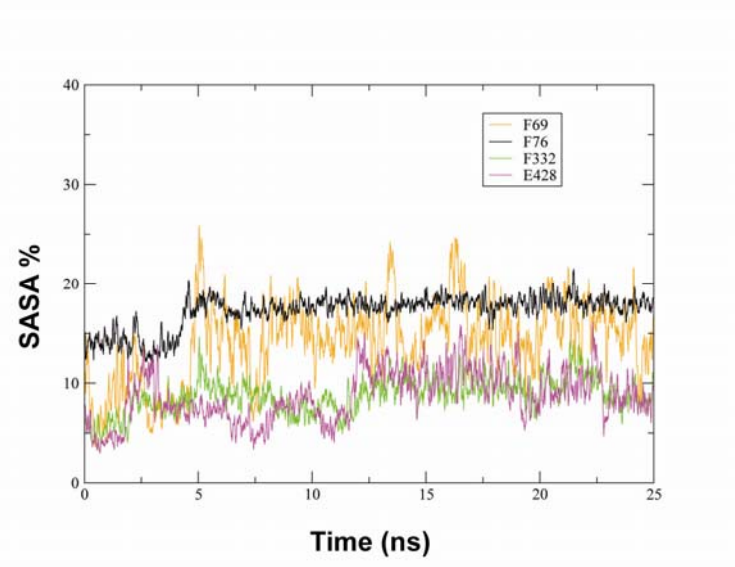

Figure S3. Spearman's rank test on dihedrals of the aromatic cluster residues during intracellular pulling.

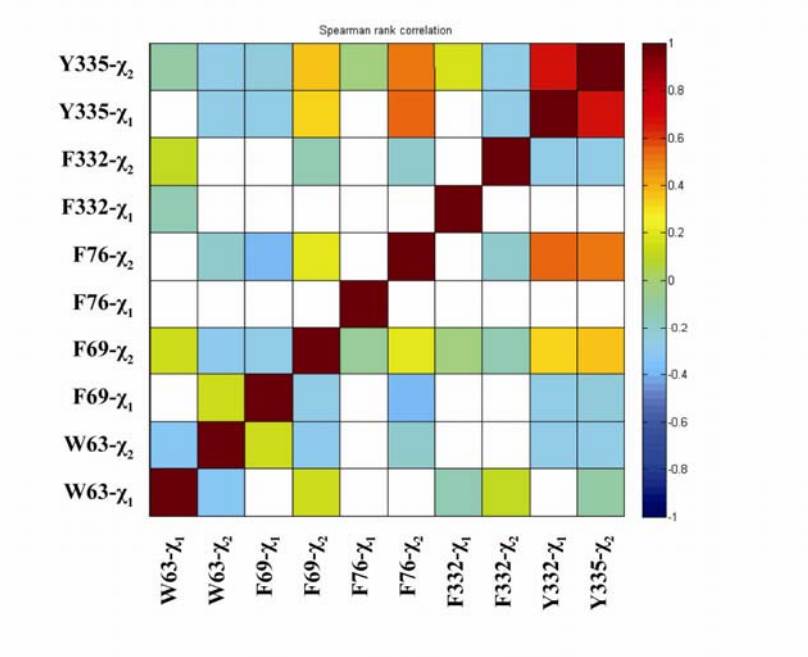

White indicates a P-value greater than 0.0001 (not significant).

Figure S4. Residue-based RMSD of the inward-facing conformation to S1-DAT by RMSDTT.

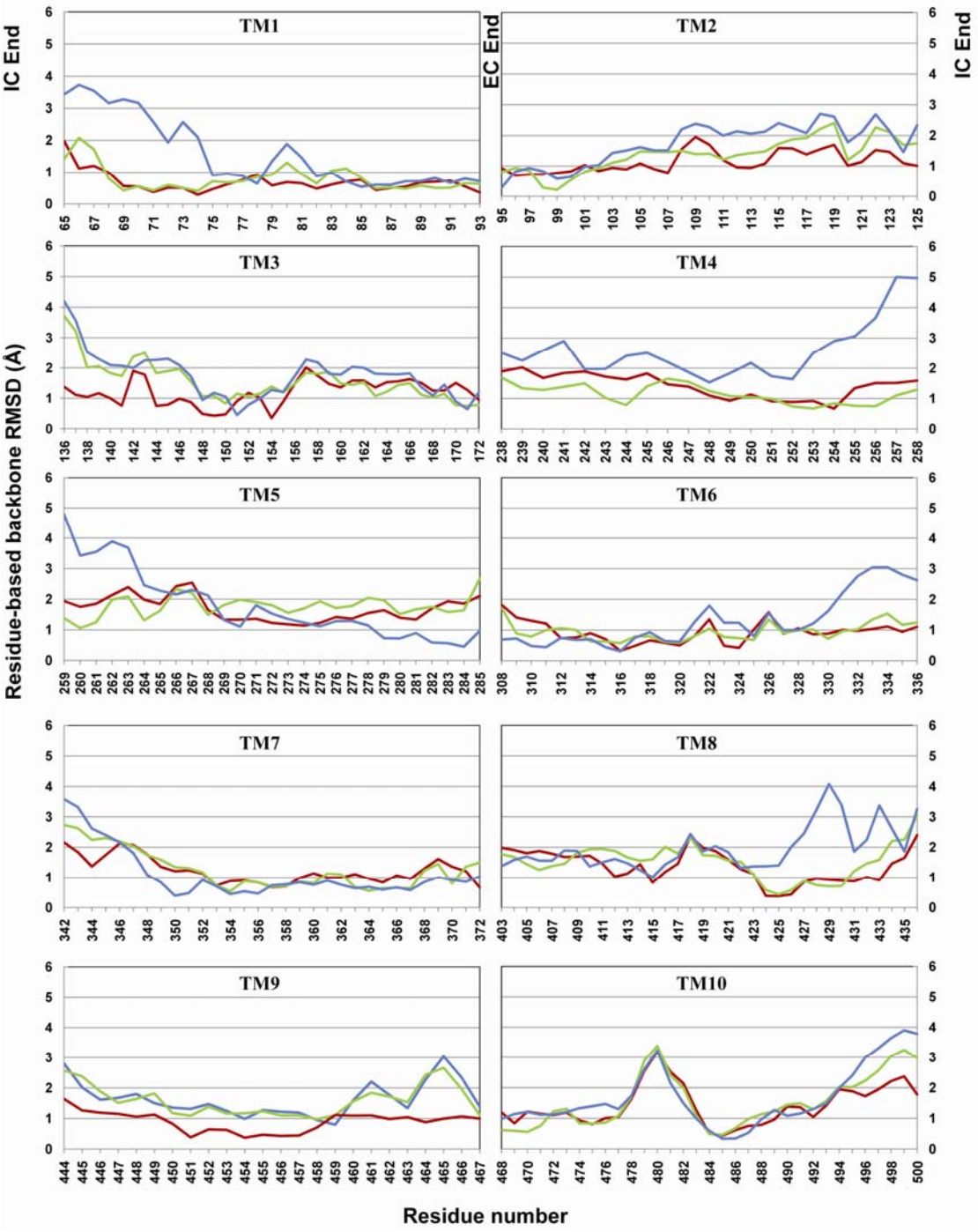

The model of DAT after substrate has moved from the S1 site to the extracellular side (shown in red); the S1,S2-DAT construct (in blue), and the inward-facing conformation (green) were aligned to S1-DAT using RMSDTT [2] and RMSD values were plotted for residues in TM1 to TM10.

Table S1. Rotamer changes from S1-DAT to S1,S2-DAT.

Residue	Dihedrals	S1-DAT [a]				S1,S2-DAT [b]			
		Average [c]	trans % [d]	g+ % [d]	g- % [d]	Average [c]	trans % [d]	g+ % [d]	g- % [d]
F76$^{1.42}$	φ	-59.7				-68.6			
L80$^{1.46}$	φ	-75.6				-60.6			
	ψ	-27.9				-34.8			
	χ_2	n/a	95.4	1.5	0	n/a	83.6	4.3	0.7
W84$^{1.50}$	ψ	-47.3				-52.5			
F155$^{3.49}$	φ	-64.3				-72.5			
	ψ	-44.1				-34.1			
	χ_1	188.9		0	0		35.2	54.5	0
	χ_2	44.0				30.4			
Y156$^{3.50}$	χ_1	-137.2				-66.5			
	χ_2	104.2				138.1			
S262$^{5.40}$	χ_1	n/a	55.1	0	40		66.4	24.5	0
F320$^{6.53}$	χ_2	66.4				14.5			
F332$^{6.65}$	χ_1	-75.5				-82.6			
	χ_2	-171.8				-165.0			
L418$^{8.56}$	φ	-69.3				-76.7			
	ψ	-18.0				112.6			
	χ_1	-55.3	0	0	96.5	n/a	85.3	0	11.3
	χ_2	181.6	98.3	0	0	n/a	7.9	88.2	0
M424$^{8.62}$	χ_1	n/a	61.6	3.7	20.4	n/a	35.6	0	52.8
	χ_2	n/a	62.1	16.4	6.4	n/a	89.2	1.2	0

[a,b] Dihedral angles were calculated using the last 5 ns of equilibration trajectories of S1-DAT (the 12th – 16th ns) [a] and S1,S2-DAT (the 21st – 25th ns) [b], respectively. Snapshots were extracted every 5 ps.

[c,d] If the dihedrals are continuous in the 5 ns simulation, averages are calculated; otherwise, the percentage of trans, g-, g+ [d] were reported, which are defined as within ±25 degrees of 180, -60 and +60 degrees, respectively.

Table S2. Dihedrals of the aromatic cluster in different conformational states of DAT.

Residues	Dihedrals	S1-DAT [a]	S1,S2-DAT [b]	Inward-facing [c]
W63$^{1.29}$	φ	-69.4	-75.1*	-89.3*
	ψ	-56.9	-89.2*	-91.1*
	χ_1	-58.9	-69.0*	-57.8
	χ_2	82.7	100.7*	111.2*
F69$^{1.35}$	φ	-69.5	-70.6	-78.5*
	ψ	-44.6	-49.2	-54.0*
	χ_1	185.0	182.3	188.7
	χ_2	62.7	54.9*	235.1*
F76$^{1.42}$	φ	-59.7	-69.6*	-82.0*
	ψ	-44.5	-47.0	-45.1
	χ_1	181.9	176.9	184.2
	χ_2	71.2	73.5	75.7
F332$^{6.65}$	φ	-61.8	-62.9	-62.1
	ψ	-48.4	-47.8	-47.3
	χ_1	-75.7	-82.6*	193.5*
	χ_2	-171.8	-165.0*	83.5*
Y335$^{6.68}$	φ	-74.2	-76.8	-75.9
	ψ	-21.6	-6.67*	-18.4
	χ_1	-69.9	-75.2*	193.7*
	χ_2	104.9	117.3*	-86.8*[d]
E428$^{8.66}$	φ	-58.8	-61.9	-64.2*
	ψ	-44.8	-40.5	-47.8
	χ_1	182.6	184.5	182.8
	χ_2	64.1	58.9*	177.7*

[a,b,c] Dihedral angles were calculated using the last 5 ns of equilibration trajectories of [a] S1-DAT (the 12th – 16th ns), [b] S1,S2-DAT (the 21st – 25th ns), and [c] the inward-facing conformation (the 11th – 15th ns), respectively. Dihedral were calculated on snapshots extracted every 5 ps using ptraj [30]. Average values were reported.

[*] changes more than 5 degrees compared to S1-DAT.

[d] Tyr335$^{6.88}$-χ_2 was discontinuous with 8.2% trans, 8.2% g- , and 8.7% g+. 8.2%, g+ 8.7%. Trans, g-, g+ were defined as within ±25 degrees of 180, -60 and +60 degrees, respectively.

Table S3. RMSD for the extracellular and intracellular segments when individual TM was fitted with its extracellular segment.

	Extracellular Segments		Intracellular Segments	
	Residues	RMSD (Å)	Residues	RMSD (Å)
TM1	$L80^{1.46}$ – $N93^{1.59}$	0.4	$K65^{1.31}$ – $D79^{1.45}$	4.4
TM2	$G95^{2.33}$ – $P101^{2.39}$	0.7	$Y102^{2.40}$ – $R125^{2.63}$	6.3
	$Y102^{2.40}$ – $M111^{2.49}$	0.5	$P112^{2.50}$ – $R125^{2.63}$	2.9
TM3	$F154^{3.48}$ – $T172^{3.66}$	0.6	$P136^{3.30}$ – $G153^{3.47}$	3.1
TM4	$W238^{4.45}$ – $F253^{4.60}$	0.7	$S254^{4.61}$ – $G258^{4.65}$	3.8
TM5	$A270^{5.47}$ – $V285^{5.62}$	0.5	$V259^{5.35}$ – $T269^{5.46}$	3.2
TM6	$A308^{6.41}$ – $L322^{6.55}$	0.4	$V328^{6.61}$ – $N336^{6.69}$	2.6
TM7	$S354^{7.39}$ – $A373^{7.58}$	0.7	$M342^{7.26}$ – $S354^{7.39}$	1.2
TM8	$L403^{8.37}$ – $D421^{8.59}$	0.9	$S422^{8.60}$ – $D436^{8.74}$	3.7
TM9	$T456^{9.49}$ – $N466^{9.59}$	0.5	$H444^{9.37}$ – $A455^{9.48}$	1.1
TM10	$G468^{10.40}$ – $F478^{10.50}$	0.6	$A479^{10.51}$ – $G500^{10.73}$	3.4
TM11	$S528^{11.49}$ – $F543^{11.64}$	0.5	$L518^{11.39}$ – $V527^{11.48}$	1.2
TM12	$D555^{12.31}$ – $S568^{12.45}$	0.6	$M569^{12.46}$ – $G585^{12.62}$	3.3

Text S1. Supporting Methods

Spearman's' Test – Spearman's test was carried out using R.

Calculation of difference distance matrix map (DDMP) – The mass-weighted distance matrix was calculated with ptraj in AMBER9 [1] on snapshots saved every 5 ps during the last 5 ns of equilibration trajectories of S1-DAT and S1,S2-DAT, respectively. The DDMP was generated by subtracting distances in S1-DAT from S1,S2-DAT, and plotted with Matlab 2007b (The MathWorks, Inc.).

Individual TM alignments using their extracellular segments to identify local TM distortions – The local conformational changes in TM11 and TM2 were not addressed in this study due to the poor homology between LeuT and DAT. In addition, TM11 and TM12 do not belong to the 10-TM functional core of NSSs. Except for TM11 and TM12, each TM in the inward-facing conformation of DAT was superimposed individually on the corresponding TM in S1-DAT using backbone atoms of residues in the extracellular segment. The extracellular segments of TMs were defined arbitrarily based on their residue-based RMSD from global alignment as follows: TM1, $L80^{1.46}$ –$N93^{1.59}$; TM2, $G95^{2.33}$ - $P101^{2.39}$; TM3, $F154^{3.48}$ – $T172^{3.66}$; TM4, $W238^{4.45}$ – $F253^{4.60}$; TM5, $A270^{5.47}$ – $V285^{5.62}$; TM6, $A308^{6.41}$ – $L322^{6.55}$; TM7, $S354^{7.39}$ – $A373^{7.58}$; TM8, $L403^{8.37}$ – $D421^{8.59}$; TM9, $T456^{9.49}$ – $N466^{9.59}$; TM10, $G468^{10.40}$ – $F478^{10.50}$; TM11, $S528^{11.49}$ – $F543^{11.64}$; and TM12, $D555^{12.31}$ – $S568^{12.45}$. No local conformational changes were identified in TM7 and TM9.

References

1. Case DA, Darden, T.A., Cheatham, III, T.E., Simmerling, C.L. , Wang, J., et al. (2006) AMBER 9. University of California, San Francisco.

The Substrate-driven Transition to an Inward-facing Conformation in the Functional Mechanism of the Dopamine Transporter

Jufang Shan, Jonathan A Javitch, Lei Shi and Harel Weinstein

Text S2. Hinge regions underlie local and global conformational changes

TM1

The unwound regions in TMs1 and 6 had been postulated to be ligand-related hinges, and TM1a and TM1b have been proposed to move during the conformational transition associated with the translocation cycle [1]. In DAT, the unwound region in TM1 consists of two residues V78$^{1.44}$ and D79$^{1.45}$, and divides TM1 into two helical segments TM1a and TM1b. This unwound region contributes to the S1 site and coordinates both bound Na^+ ions: D79$^{1.45}$ forms a salt bridge with the protonated amine of DA and coordinates Na1, and the backbone carbonyl of V78$^{1.44}$ coordinates Na2. In the globally aligned inward-facing DAT, TM1a exhibits a significant rearrangement that registers a large residue-based RMSDs of nearly 4 Å relative to S1-DAT. Notably, away from the N-terminus the residue-based RMSD decreases to 1 Å at position G75$^{1.41}$ (a half-turn before the unwound region) and remains close to 1Å for residues in TM1b (Figure S4 in File S1). Therefore, in the globally aligned models, the cytoplasmic TM1a in the inward-facing conformation is seen to be shifted outwards with the unwound region serving as a hinge (Figure S5A in File S2).

To examine whether the conformational change in TM1 was caused by local change in TM1 itself or by the global alignment method, we fitted the backbones of the immobile extracellular section

from L80$^{1.46}$ to N93$^{1.59}$ in the inward-facing conformation to those of S1-DAT. A small RMS of 0.4 Å is found this way for the fitted extracellular section, whereas the intracellular section registers a big RMS of 4.4 Å (Table S3 in File S1). The conformational change observed in this way (Figure S5B in File S2) is similar to the change seen when the two conformations were aligned using the whole protein with the RMSDTT method [2].

To quantify further the structural change in TM1, the helix kink was quantified with a ProKink calculation performed at position L80$^{1.46}$, after the unwound region. Compared to S1-DAT the bend angle of this helix in the inward-facing conformation changed by 6 degrees, and the face shift altered by 40 degrees (Table 5). Residues around the unwound region are important for the translocation cycle even if they are not directly involved in binding S1 and Na^+, as evidenced by the findings that mutations G94$^{1.41}$C, A96$^{1.43}$C and L99$^{1.46}$C in hSERT [3], and G59$^{1.41}$C, I62$^{1.44}$C and L64$^{1.46}$C in GAT-1, decrease substrate uptake [4]. All these functionally important positions 1.41, 1.43, 1.44 and 1.46 are highly conserved in NSSs [5].

TM2

The two highly conserved [5] and functionally important prolines in TM2 are P101$^{2.39}$ and P112$^{2.50}$. P101$^{2.39}$A mutation in rDAT decreases DA uptake affinity and the V_{max} of DA transport [6,7], and increases efflux [8]. The P101$^{2.39}$C mutation in hDAT decreases K_m for tyramine uptake [9]; P97$^{2.39}$C in hNET decreases apparent affinity for cocaine, and increases K_D and B_{max} of ^{3}H-nisoxetine [10]. P112$^{2.50}$A in rDAT decreases DA uptake affinity and the V_{max} of DA transport [6,7]. The mutants P112$^{2.50}$C in DAT [9], and P131$^{2.50}$C in rSERT are completely inactive [11]; P108$^{2.50}$C in hNET decreases uptake of ^{3}H-noradrenaline and ^{3}H-nisoxetine binding [10]. Considering the functional impact of these mutations and the kinks these two prolines introduced in TM2, we proposed earlier that a pincer-like configuration in TM2 and the flexibility introduced by P101$^{2.39}$ and P112$^{2.50}$ are important to the interconversion between S1-DAT and the inward-facing conformation [9]. Indeed,

we find here that these two prolines change the direction of the helix axis of TM2 twice, separating TM2 into three segments: the extracellular one N-terminal to P101$^{2.39}$, the one between these two prolines, and the intracellular one C-terminal to P112$^{2.50}$. These three segments exhibited different global conformational rearrangements when DAT transited from S1-DAT to the inward-facing conformation (Figure S5A, C, D in File S2). In particular, the extracellular segment containing the glycine at the N-terminus of TM2 moved towards EL3, whereas the middle segment tilted outwards together with the intracellular segment. Fitting TM2 using either the first or second helical segment also showed that TM2 rearranged and distortions were observed around the two prolines. Indeed, the bend angles at P101$^{2.39}$ and P112$^{2.50}$ changed significantly in the transition from S1-DAT to the inward-facing conformation, by 7 and 5 degrees, respectively (Table 5).

The global conformational change in the N-terminus of TM2 is associated with that of the EL1 loop. The highly conserved NGGGAF motif in EL1-TM2 moved towards EL3, a change that is consistent with findings in the literature. Several mutational studies suggest that EL1 undergoes conformational change during translocation cycle in GLYT2a [12] and SERT [11], and is required to maintain transport activity in GAT-1 [13] and rSERT [14]. In addition, Yamashita et al. proposed that in the conformational transition during the translocation cycle, the movement in TM1 may be accompanied by a conformational change in the linker between TM1 and TM2 [1]. Indeed, the NGGGAF motif in LeuT moved towards EL3 when transiting from the occluded conformation to an open-to-out conformation, TM1b and TM2 swings outwards and there is local conformational change in the NGGGAF motif [15].

TM3

TM3 is involved in ligand binding in both S1 (S149$^{3.43}$, V152$^{3.46}$, T156$^{3.50}$) and S2 (F155$^{3.49}$, I159$^{3.53}$, W162$^{3.56}$), and also lines the extracellular translocation pathway (G153$^{3.47}$, N157$^{3.51}$, I160$^{3.54}$, A163$^{3.57}$). In the globally alignment of the inward-facing conformation to S1-DAT, the extracellular

segment of TM3 appears to have moved slightly inwards due to interactions with S2 (Figure 5A in File S2), whereas its intracellular segment (together with that of TM12) moved inwards to remain associated with the rest of the transporter (Figure S6 in File S2). The intracellular segment of TM3 moved in somewhat toward the place originally occupied by TM6, but the H-bond between S149$^{3.43}$ and the carbonyl of F326$^{6.59}$ was maintained during the transition. In contrast, due to rotamer changes in Y151$^{3.45}$, the H-bond between Y151$^{3.45}$ and A565$^{12.42}$ broke although TM3 and TM12 moved inwards together (Figure S6A, B in File S2).

Residue-based RMSDs calculated with RMSDTT for the alignment of the two conformations identifies a hinge region in the middle of TM3 (Figure S4 in File S1). This was further confirmed by aligning the extracellular segment of TM3, which shows that the intracellular segment underwent rearrangement with an RMSD of 3.1 Å whereas the extracellular segments are only 0.6 Å apart by RMSD (Table S3 in File S1). Here, the hinge region contains two helix-disrupting residues S149$^{3.43}$ and G153$^{3.47}$. The bend angles of TM3 changed significantly at these two residues during the conformational transition, by 8 and 9 degrees, respectively (Table 5). Mutation studies suggest that this hinge region is functionally important, as the V141$^{3.43}$C, Y143$^{3.45}$C and N145$^{3.47}$C mutations in the creatine transporter reduce uptake [16] and W135$^{3.45}$S in mouse GAT reduces GABA transport [17]. Considering the structural flexibility and functional importance of this region, we hypothesize that this hinge region is involved in the conformational transition associated with the translocation cycle.

TMs 4 and 5

TMs 4 and 5 are at the outer rim of the transmembrane domain. They form a V-shaped structure wrapping around TMs3 and 8. During intracellular pulling of DA in the SMD simulation, the ligand exits from a channel formed by TMs 1, 5, 6 and 8 (Figure 5B in File S2) when TMs1, 5 and 8 move outwards; TM6 also moves outwards but in an opposite direction, to open the channel. TM4, whose intracellular segment neighbors that of TM8, also moved outwards and also shifted up along the helix

axis about one residue (~1/4 turn). The upwards shift explains the relatively large residue-based RMSD of the extracellular segment (~2–3 Å) compared to other extracellular segments (Figure S4 in File S1). Fitting the extracellular segment of TM4 clearly showed that residue S254$^{4.61}$ was at the hinge region of TM4 (Figure S5E in File S2). The bend angle of TM4 changed 12 degrees at this functionally important position (Table 5). S253$^{4.61}$A in rDAT [18] and C228$^{4.61}$S in GAT-1 [19] reduce transport activity; S253$^{4.61}$A together with Y251$^{4.59}$A in rDAT also reduces the affinity for CFT but increases the affinity for DA [20].

In the superposition, we observed large residue-based RMSDs for the intracellular portion of TM5 (up to 6 Å) but only around 1 Å for the extracellular segment (Figure S4 in File S1). Aligning the extracellular portion of TM5 in the inward-facing state to that in S1-DAT, showed the global and local rearrangement (Figure S5F in File S2) to have similar patterns, confirming a local distortion in the middle of TM5. A helix-disrupting residue T269$^{5.46}$ played a role in the rearrangement of TM5, and ProKink analysis showed that the bend angle at T269$^{5.46}$ changed by 10 degrees in the transition from S1-DAT to the inward-facing conformation. Notably, two conserved helix-disrupting residues, T271$^{5.48}$ and P273$^{5.50}$, are located half-turn and one turn after T269$^{5.46}$, respectively, and might coordinate T269$^{5.46}$ in the rearrangement of TM5. The coordination between threonine and proline has been reported before in a functional important T*X*P motif that introduces a bend in TM2 of CCR5 [21]. Interestingly, the three residues T269$^{5.46}$, T271$^{5.48}$ and P273$^{5.50}$ were found to be important for the translocation cycle in studies showing that both T284$^{5.46}$C and T286$^{5.48}$C in SERT decrease K_m and increase V_{max} for 5-HT transport [22]. T268$^{5.48}$A in hNET affects the affinities for different ligands differently [23]; P273$^{5.50}$A in rDAT reduces the K_m values of DA efflux and the apparent velocities of DA efflux [7], the V_{max} of DA uptake, and the affinities for both DA and WIN 35428 binding [6]. Although functionally important, positions 5.46 and 5.50 are not conserved between prokaryotic and

eukaryotic NSSs. In LeuT, 5.46 is an alanine and 5.50 is a leucine. However the structural role of these two residues might be mimicked by Pro200$^{5.48}$ in LeuT, which could give LeuT the structural flexibility it needs during the conformational transition we studied.

TM6

Like in TM1, the unwound region (G323$^{6.56}$–V324$^{6.57}$–G325$^{6.58}$–F326$^{6.59}$–G327$^{6.60}$) in TM6 participates in S1 ligand binding, with F326$^{6.59}$ in direct contact with DA. The nature of the conformational rearrangement in TM6 associated with the transition from S1-DAT to the inward-facing conformation is also similar to that in TM1: not much movement of the extracellular segment and the unwound region, but more in the intracellular segment TM6b (Figure S7 in File S2), with residue-based RMSDs going up to 3 Å in TM6b (Figure S4 in File S1). Superposition of the TM6a segments (A308$^{6.41}$ – L322$^{6.55}$) of the two conformations reveals a small backbone RMS of 0.6 Å, but a bigger one for TM6b (V328$^{6.61}$ – Y335$^{6.68}$), 2.6 Å (Figure S7 in File S2). The C_α atom of Y335$^{6.68}$ in the inward-facing conformation shifted outwards by 3.1 Å from that of S1-DAT, breaking the H-bond between the backbone carbonyl of G327$^{6.60}$ and the sidechain hydroxyl of S429$^{8.67}$ broke (Figure S7A,B in File S2). The movement of TM6b away from TM8, TM4 and TM5 adds to the opening of the channel in the center of the intracellular portion of DAT, allowing DA to exit (Figure S7B in File S2). This is consonant with the observation that residues in the unwound region are functionally important even if they do not bind the ligand in S1: G323$^{6.56}$V in hDAT completely blocks tyramine uptake; P339$^{6.57}$L in hSERT decreases transport activity [24]; L298$^{6.57}$C in rGAT reduces GABA uptake [25]; and G327$^{6.60}$V in hDAT greatly decreases plasma membrane expression and completely blocks substrate transport [26].

TM8

TM8 is one of the two TMs that participate in ligand binding in S1 and in lining both the extracellular and intracellular translocation pathways; the other one is TM1. TM8 is also one of the few

TMs whose extracellular segments were found to undergo global conformational changes during the transition (Figure 5A in File S2). While its extracellular portion bent outwards, its intracellular portion also bent outwards towards TM4, 5 and 9 (Figure 5B in File S2). As a result, both the extracellular and cytoplasmic ends of TM8 have large residue-based RMSDs of around 3 Å (Figure S4 in File S1) and a hinge region at the middle of the helix. The hinge region contains a S1 binding residue, $S422^{8.60}$, which H-bonds one of the hydroxyl groups in DA. ProKink analysis shows that the face shift in TM8 changed by 44 degrees at $S422^{8.60}$ (Table 5). Considering that $S422^{8.60}$ is involved in S1 ligand binding and conformational transition, it is not surprising that mutating this serine to alanine decreases DA uptake [18], and mutating to threonine or cysteine in GAT-1 increases K_m for GABA transport and leads to lithium leak currents [27].

TM10

In the TM10 of DAT, there is a "melted" region consisting of the four residues $A480^{10.52}$–$G481^{10.53}$–$T482^{10.55}$–$S483^{10.56}$. This region is not conserved [5], and only one out of the four positions, 10.53, is conserved with helix-disrupting residues Gly/Pro/Thr/Ser/Cys. The other three positions have deletion mutations, e.g., position 10.54 in DAT and positions 10.55 and 10.56 in Tyt1 and TnaT. The extracellular segment N-terminal to, and the intracellular segment C-terminal to this melted region exhibited different global rearrangement when DAT converted from S1-DAT to inward-facing conformations (Figure S5G in File S2). In the extracellular portion one small movement were observed, with residue-based RMSDs of about 1 Å, whereas the intracellular one moved significantly outwards with RMSDs of up to 4 Å (Figure S4 in File S1). The melted region itself also had large RMSDs, likely caused by the lack of secondary structure. Fitting the extracellular segment of TM10 in the two conformations illustrates the TM rearrangement (Figure S5G in File S2). The significant movement in the intracellular TM segment was generated by changes in bend angle at $G481^{10.53}$ (from 32 to 37 degree) and the face shift at $S483^{10.56}$ (from 137 to 81 degree). Despite the lack of conservation, this

melted region is functional important as shown by findings that mutation of both 10.55 and 10.56 in rDAT [20], and mutation of 10.56 in hSERT [28,29] affect ligand binding as well as substrate uptake.

Figure S5. Global and local conformational changes of individual TMs.

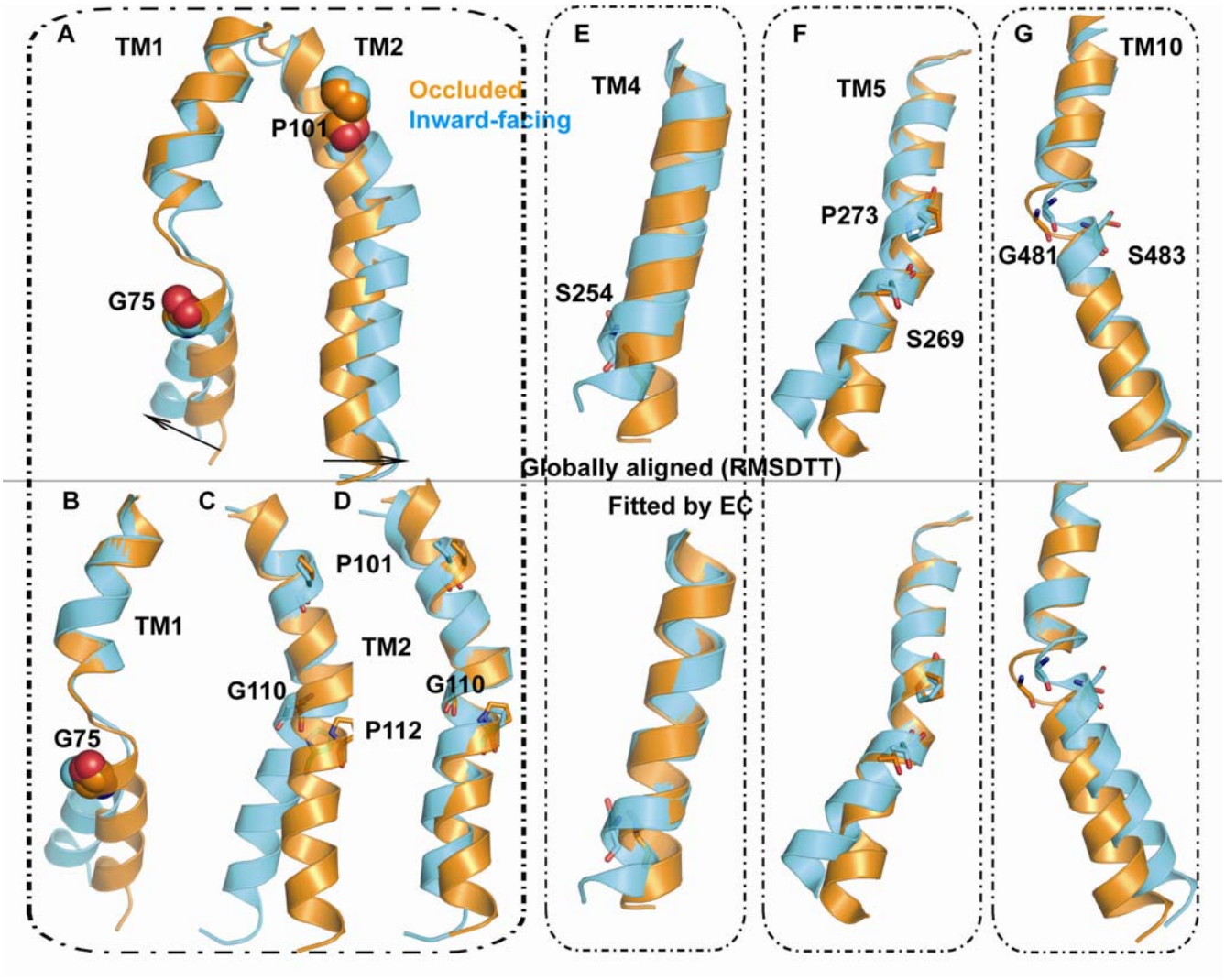

Top panels show global conformational changes from S1-DAT (orange) to the inward facing conformation (cyan) (whole structures were aligned using RMSDTT [2]; the bottom panels show local conformational changes (individual EC segments are aligned as detailed below). (**A**) Global conformational changes in TMs1 and 2. The rearrangements in the EC segments are small while the IC segments starting from the hinge residues ($G75^{1.41}$ and $P101^{2.39}$, in spheres) underwent larger-scale movements.

(**B**–**D**) Local conformational changes in TM1 (**B**) and TM2 (**C**,**D**). TM1 in the inward-facing conformation was fitted to TM1 in S1-DAT using the extracellular segment $L80^{1.46}$ – $N93^{1.59}$. TM2 was fitted to its counterpart using the extracellular segment $G95^{2.33}$ – $P101^{2.39}$ (**C**) or the middle segment $Y102^{2.40}$ – $M111^{2.49}$ (**D**).

(**E**–**G**) Conformational changes in TM4 (**E**), TM5 (**F**) and TM10 (**G**). In bottom panels, individual EC segments were fitted using the following residues: TM4, $W238^{4.45}$ – $F253^{4.60}$; TM5, $A270^{5.47}$ – $V285^{5.62}$; and TM10, $G468^{10.40}$ – $F478^{10.50}$. Hinge residues $G75^{1.41}$, $P101^{2.39}$, $G110^{2.48}$ and $P112^{2.50}$, $S254^{4.61}$, $S269^{5.46}$ and the unwound region $G481^{10.53}$ and $T483^{10.56}$ are shown in spheres or sticks.

Figure S6. Conformational changes associated with the intracellular segment of TM3.

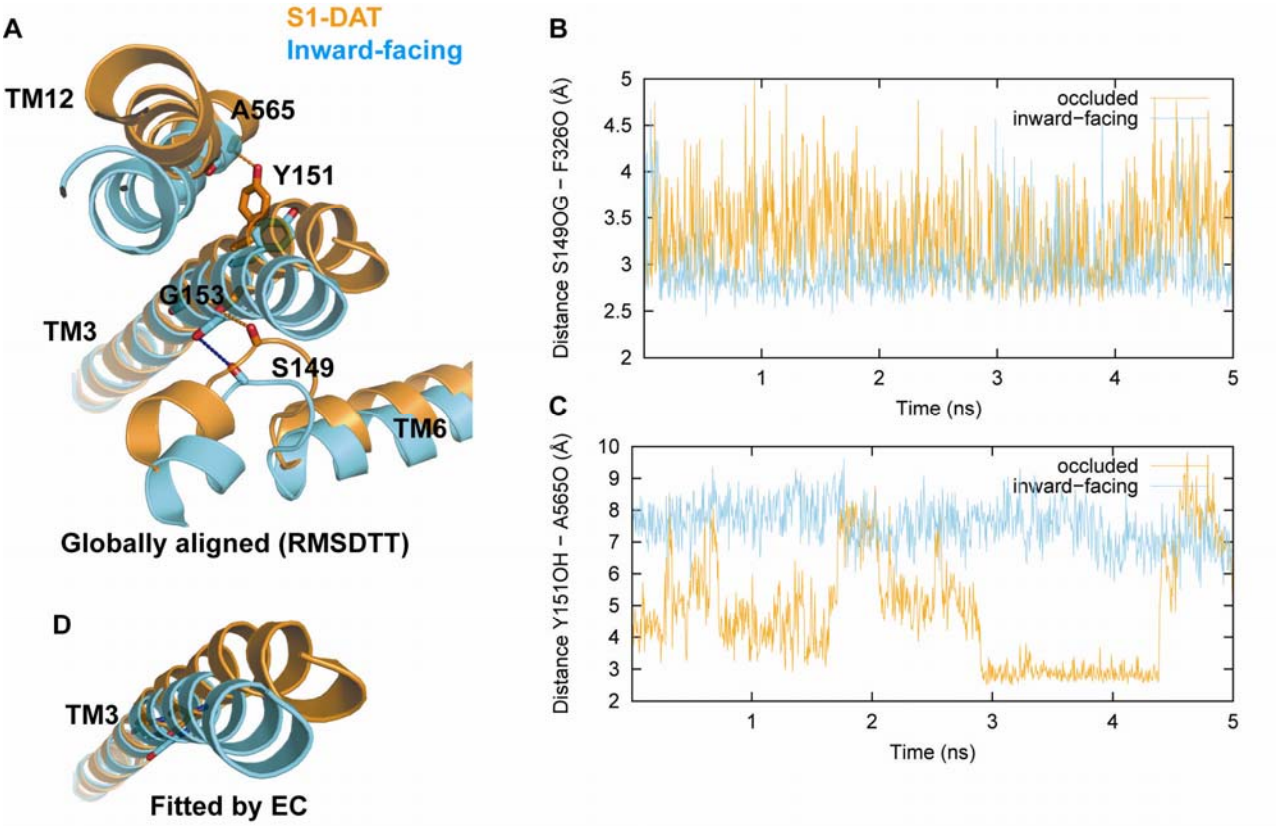

(**A**) Conformational changes in TM3, 6 and 12 from S1-DAT (orange) to the inward-facing conformation (cyan). DAT was aligned with RMSDTT using the entire protein. The intracellular segment of TM3 moved to the place originally occupied by TM6, and TM12 moves toward TM3. The H-bond between S149$^{3.43}$ and F326$^{6.59}$ is maintained (**B**); the one between A565$^{12.42}$ and Y151$^{3.45}$ is broken (**C**).

(**D**) TM3 in the inward-facing conformation is fitted to that in the occluded conformation using the extracellular segment F154$^{3.48}$ – T172$^{3.66}$.

Figure S7. Conformational changes associated with TM6.

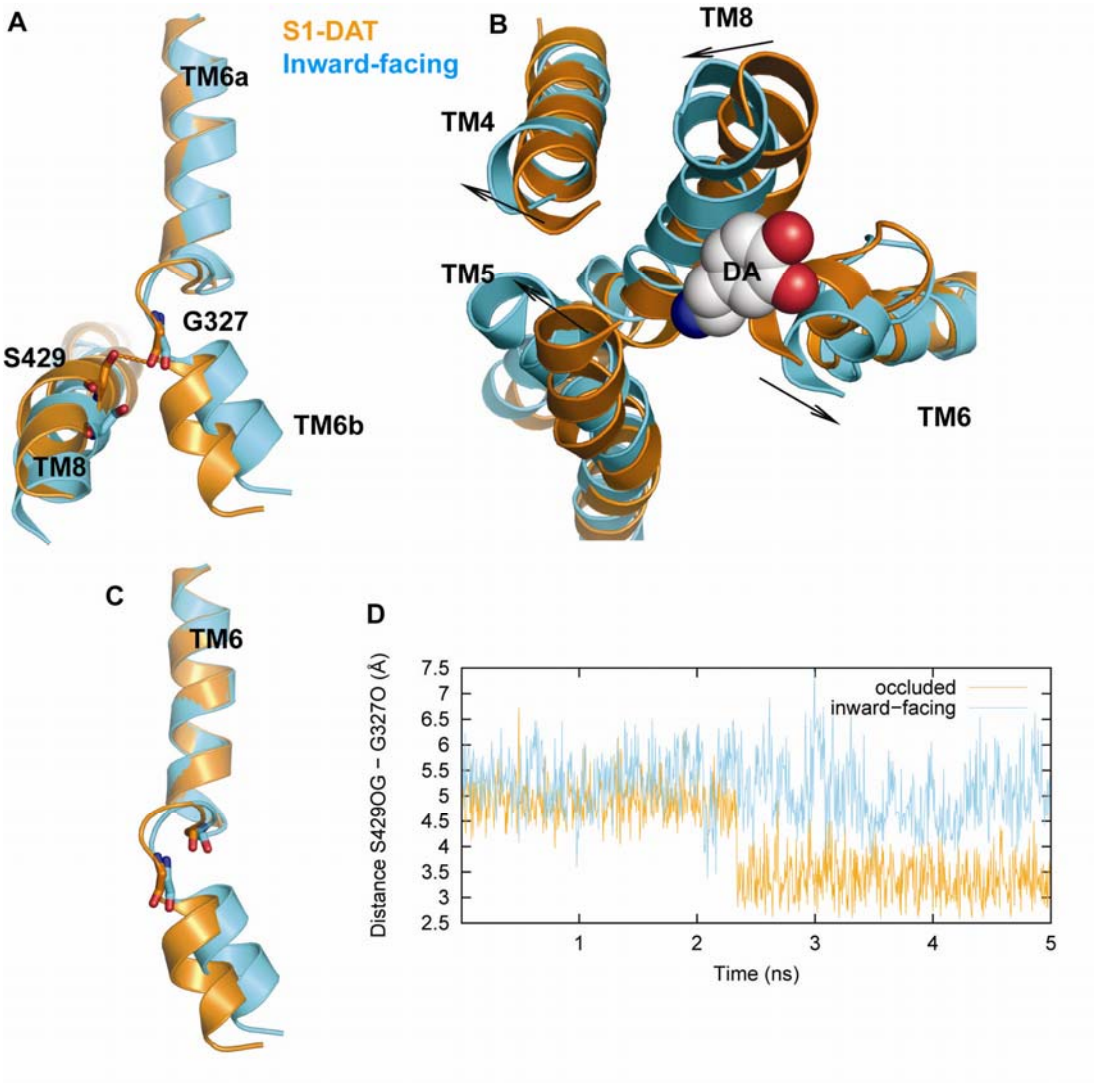

(**A**) TM6b moved away from TM8 in the inward-facing conformation (cyan) compared to S1-DAT (orange). The H-bond between G327$^{6.60}$ and S429$^{8.67}$ is broken (**D**). DAT was aligned with RMSDTT using the whole structure.

(**B**) The intracellular segments of TMs4, 5, and 8 moved outward and that of TM6 moved outward in the opposite direction, creating space for the exiting DA substrate molecule.

(**C**) TM6 in the inward-facing conformation is fitted to that in S1-DAT with the EC segment A308$^{6.41}$ –

L322$^{6.55}$. (**D**) The distances between the carboxyl oxygen of S429$^{8.67}$ and the carbonyl oxygen of G327$^{6.60}$ in S1-DAT (orange) and the inward-facing conformation (cyan).

References

1. Yamashita A, Singh SK, Kawate T, Yan Jin Y, Gouaux E (2005) Crystal structure of a bacterial homologue of Na^+/Cl^- dependent neurotransmitter transporters. Nature 437: 215-223.

2. Gracia L (2005) RMSDTT: RMSD Trajectory Tool. 2.5 ed. Weill Medical College of Cornell University, Department of Physiology and Biophysics.

3. Henry LK, Adkins EM, Han Q, Blakely RD (2003) Serotonin and cocaine-sensitive inactivation of human serotonin transporters by methanethiosulfonates targeted to transmembrane domain I. J Biol Chem 278: 37052-37063.

4. Zhou Y, Bennett ER, Kanner BI (2004) The aqueous accessibility in the external half of transmembrane domain I of the GABA transporter GAT-1 Is modulated by its ligands. J Biol Chem 279: 13800-13808.

5. Beuming T, Shi L, Javitch JA, Weinstein H (2006) A comprehensive structure-based alignment of prokaryotic and eukaryotic neurotransmitter/Na+ symporters (NSS) aids in the use of the LeuT structure to probe NSS structure and function. Mol Pharmacol 70: 1630-1642.

6. Lin Z, Itokawa M, Uhl GR (2000) Dopamine transporter proline mutations influence dopamine uptake, cocaine analog recognition, and expression. FASEB J 14: 715-728.

7. Itokawa M, Lin Z, Uhl GR (2002) Dopamine efflux via wild-type and mutant dopamine transporters: alanine substitution for proline-572 enhances efflux and reduces dependence on extracellular dopamine, sodium and chloride concentrations. Brain Res Mol Brain Res 108: 71-80.

8. Lin Z, Uhl GR (2005) Proline mutations induce negative-dosage effects on uptake velocity of the dopamine transporter. J Neurochem 94: 276-287.

9. Sen N, Shi L, Beuming T, Weinstein H, Javitch JA (2005) A pincer-like configuration of TM2 in the human dopamine transporter is responsible for indirect effects on cocaine binding. Neuropharmacology 49: 780-790.

10. Sucic S, Bryan-Lluka LJ (2005) Roles of transmembrane domain 2 and the first intracellular loop in human noradrenaline transporter function: pharmacological and SCAM analysis. J Neurochem 94: 1620-1630.

11. Sato Y, Zhang YW, Androutsellis-Theotokis A, Rudnick G (2004) Analysis of transmembrane domain 2 of rat serotonin transporter by cysteine scanning mutagenesis. J Biol Chem 279: 22926-22933.

12. Lopez-Corcuera B, Nunez E, Martinez-Maza R, Geerlings A, Aragon C (2001) Substrate-induced conformational changes of extracellular loop 1 in the glycine transporter GLYT2. J Biol Chem 276: 43463-43470.

13. Zhou Y, Kanner BI (2005) Transporter-associated currents in the gamma-aminobutyric acid transporter GAT-1 are conditionally impaired by mutations of a conserved glycine residue. J Biol Chem 280: 20316-20324.

14. Mao Y, Mathewson L, Gesmonde J, Sato Y, Holy M, et al. (2008) Involvement of serotonin transporter extracellular loop 1 in serotonin binding and transport. Mol Membr Biol 25: 115-127.

15. Singh SK, Piscitelli CL, Yamashita A, Gouaux E (2008) A Competitive Inhibitor Traps LeuT in an Open-to-Out Conformation. Science 322: 1655-1661.

16. Dodd JR, Christie DL (2005) Substituted cysteine accessibility of the third transmembrane domain of the creatine transporter: defining a transport pathway. J Biol Chem 280: 32649-32654.

17. Kleinberger-Doron N, Kanner BI (1994) Identification of tryptophan residues critical for the function and targeting of the gamma-aminobutyric acid transporter (subtype A). J Biol Chem 269: 3063-3067.

18. Lin Z, Zhang PW, Zhu X, Melgari JM, Huff R, et al. (2003) Phosphatidylinositol 3-kinase, protein kinase C, and MEK1/2 kinase regulation of dopamine transporters (DAT) require N-terminal DAT phosphoacceptor sites. J Biol Chem 278: 20162-20170.

19. Golovanevsky V, Kanner BI (1999) The reactivity of the gamma-aminobutyric acid transporter GAT-1 toward sulfhydryl reagents is conformationally sensitive. Identification of a major target residue. J Biol Chem 274: 23020-23026.

20. Itokawa M, Lin Z, Cai NS, Wu C, Kitayama S, et al. (2000) Dopamine transporter transmembrane domain polar mutants: ΔG and ΔΔG values implicate regions important for transporter functions. Mol Pharmacol 57: 1093-1103.

21. Govaerts C, Blanpain C, Deupi X, Ballet S, Ballesteros JA, et al. (2001) The T*X*P motif in the second transmembrane helix of CCR5: A structural determinant of chemokine-induced activation. J Biol Chem: 13217-13225.

22. Zhang YW, Rudnick G (2005) Cysteine-scanning mutagenesis of serotonin transporter intracellular loop 2 suggests an alpha-helical conformation. J Biol Chem 280: 30807-30813.

23. Bryan-Lluka LJ, Bonisch H, Lewis RJ (2003) chi-Conopeptide MrIA partially overlaps desipramine and cocaine binding sites on the human norepinephrine transporter. J Biol Chem 278: 40324-40329.

24. Prasad HC, Zhu CB, McCauley JL, Samuvel DJ, Ramamoorthy S, et al. (2005) Human serotonin transporter variants display altered sensitivity to protein kinase G and p38 mitogen-activated protein kinase. Proc Natl Acad Sci U S A 102: 11545-11550.

25. Mari SA, Soragna A, Castagna M, Santacroce M, Perego C, et al. (2006) Role of the conserved glutamine 291 in the rat gamma-aminobutyric acid transporter rGAT-1. Cell Mol Life Sci 63: 100-111.

26. Hastrup H, Karlin A, Javitch JA (2001) Symmetrical dimer of the human dopamine transporter revealed by cross-linking Cys-306 at the extracellular end of the sixth transmembrane segment. Proc Natl Acad Sci U S A 98: 10055-10060.

27. Zhou Y, Zomot E, Kanner BI (2006) Identification of a lithium interaction site in the gamma-aminobutyric acid (GABA) transporter GAT-1. J Biol Chem 281: 22092-22099.

28. Keller PC, 2nd, Stephan M, Glomska H, Rudnick G (2004) Cysteine-scanning mutagenesis of the fifth external loop of serotonin transporter. Biochemistry 43: 8510-8516.

29. Plenge P, Wiborg O (2005) High- and low-affinity binding of S-citalopram to the human serotonin transporter mutated at 20 putatively important amino acid positions. Neurosci Lett 383: 203-208.